Electrochemical impedance spectroscopy of mixed conductors under a chemical potential gradient: a case study of Pt|SDC|BSCF

Wei Lai and Sossina M. Haile*

Received 14th August 2007, Accepted 6th November 2007
First published as an Advance Article on the web 5th December 2007
DOI: 10.1039/b712473b

The AC impedance response of mixed ionic and electronic conductors (MIECs) exposed to a chemical potential gradient is derived from first principles. In such a system, the chemical potential gradient induces a gradient in the carrier concentration. For the particular system considered, 15% samarium doped ceria (SDC15) with $Ba_{0.5}Sr_{0.5}Co_{0.8}Fe_{0.2}O_{3-\delta}$ (BSCF) and Pt electrodes, the oxygen vacancy concentration is a constant under the experimental conditions and it is the electron concentration that varies. The resulting equations are mapped to an equivalent circuit that bears some resemblance to recently discussed equivalent circuit models for MIECs under uniform chemical potential conditions, but differs in that active elements, specifically, voltage-controlled current sources, occur. It is shown that from a combination of open circuit voltage measurements and AC impedance spectroscopy, it is possible to use this model to determine the oxygen partial pressure drop that occurs between the gas phase in the electrode chambers and the electrode|electrolyte interface, as well as the interfacial polarization resistance. As discussed in detail, this resistance corresponds to the slope of the interfacial polarization curve. Measurements were carried out at temperatures between 550 and 650 °C and oxygen partial pressure at the Pt anode ranging from 10^{-29} to 10^{-24} atm (attained using H_2/H_2O/Ar mixtures), while the cathode was exposed to either synthetic air or neat oxygen. The oxygen partial pressure drop at the anode was typically about five orders of magnitude, whereas that at the cathode was about 0.1 atm for measurements using air. Accordingly, the poor activity of the anode is responsible for a loss in open circuit voltage of about 0.22 V, whereas the cathode is responsible for only about 0.01 V, reflecting the high activity of BSCF for oxygen electro-reduction. The interfacial polarization resistance at the anode displayed dependences on oxygen partial pressure and on temperature that mimic those of the electronic resistivity of SDC15. This behavior is consistent with hydrogen electro-oxidation occurring directly on the ceria surface and electron migration being the rate-limiting step. However, the equivalent resistance implied by the oxygen partial pressure drop across the anode displayed slightly different behavior, possibly indicative of a more complex reaction pathway.

1. Introduction

Mixed oxygen ionic and electronic conductors have important applications in oxygen permeation membranes, oxygen sensors, and solid oxide fuel cells. The steady state behavior of such materials under exposure to a chemical potential gradient has been explored in several studies which either exclude[1–9] or include[10,11] a discussion of the electrolyte|electrode interfaces, with the earliest studies dating back to the classic work of Wagner.[2] In addition to this type of investigation, the behavior of mixed conductors exposed to a small signal perturbation but in a uniform chemical potential, *i.e.*, conventional impedance spectroscopy, has recently been examined by Jamnik and Maier and the present authors.[12–14] In those studies the impedance behavior is derived from first principles, and the resulting expressions are mapped to an equivalent circuit to permit physical insight into the meaning of the mathematical relationships. The validity of the approach was subsequently confirmed by the present authors in an experimental study of doped ceria.[14]

In the present work, we consider the situation in which a mixed conductor is exposed to both a chemical potential gradient and a small signal perturbation, that is, impedance spectroscopy under fuel cell conditions. We begin with the fundamental physical equations governing transport and, as in the Jamnik and Maier approach, map the expressions to an equivalent circuit. Although this circuit bears some resemblance to that derived under uniform chemical potential conditions, it contains unique elements not typically considered in phenomenological treatments of impedance spectroscopy. Moreover, it is not possible to derive an analytical expression for the impedance and we further develop numerical procedures for analyzing the experimental data.

Materials Science, California Institute of Technology, Pasadena, California, 91125. E-mail: smhaile@caltech.edu

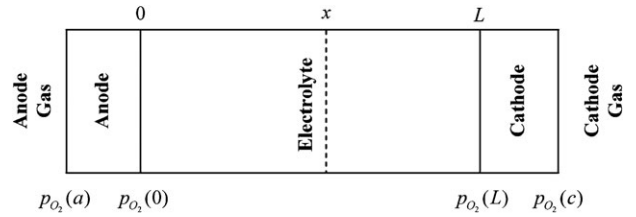

Fig. 1 Schematic of the 1-D situation under consideration, with an electrolyte placed between an anode and a cathode. The electrolyte has thickness L and contacts the anode (a) at $x = 0$ and the cathode (c) at $x = L$. The electrodes have finite (but unspecified) thicknesses. The oxygen partial pressures in the electrode chambers, $p_{O_2}(a)$ for the anode and $p_{O_2}(c)$ for the cathode, may differ from the respective values at the electrode|electrolyte interfaces.

2. Background

The physical situation, considered in one dimension, is schematically depicted in Fig. 1. The electrolyte is sandwiched between an anode (denoted "a") and a cathode (denoted "c"). The electrolyte area is A and its length L, with the anode|electrolyte interface fixed at $x = 0$, and the cathode|electrolyte interface fixed at $x = L$. The electrolyte, being a mixed ionic and electronic conductor, is taken to have two mobile species denoted "ion" for ionic species and "eon" for electronic species. In addition, the material is extrinsically doped with the dopant species, taken to be immobile and uniformly distributed through the material; furthermore, grain boundary effects are ignored, as justified below. The oxygen partial pressures within the anode and cathode chambers are experimentally fixed and denoted $p_{O_2}(a)$ and $p_{O_2}(c)$, respectively, with $p_{O_2}(a) < p_{O_2}(c)$. In such a system, oxygen potential drops are expected not only across the electrolyte, but also across the two electrodes, depending on the effectiveness of the electrode materials in catalyzing the respective electrochemical reactions. Thus, the oxygen partial pressures at the electrode|electrolyte interfaces, $p_{O_2}(0)$, and $p_{O_2}(L)$, respectively, for the interface with the anode and that with the cathode, in general, do not equal $p_{O_2}(a)$ and $p_{O_2}(c)$.

While the formalism developed in this work is applicable to any mixed conductor with one mobile ionic species and one mobile electronic species, the specific system considered here is that of acceptor doped ceria, with overall stoichiometry $Ce_{0.85}Sm_{0.15}O_{1.925-\delta}$. In this system, the mobile ionic species are oxygen ion vacancies with an effective charge of $+2$, denoted $V_O^{\bullet\bullet}$ in Kröger–Vink notation, and the mobile electronic species are electrons, e', with charge -1. The acceptor dopant species, Sm'_{Ce}, is also indicated as "A_D".

2.1 Basic equations: transport through a mixed conductor

A set of three fundamental equations govern charge transport in solids. The first is the generalized transport equation that relates the driving force (electrochemical potential) to the mass flux[15]

$$J_i^{\text{mass}}(x,t) = -\frac{\sigma_i(x,t)}{(z_i e)^2}\frac{\partial \tilde{\mu}_i(x,t)}{\partial x} \tag{1}$$

where x is position, t is time, i is the species of charge carrier, z_i is the number of charges carried by species i, e is the electron charge, $J_i^{\text{mass}}(x,t)$ is the carrier mass flux, $\sigma_i(x,t)$ is the electrical conductivity and $\tilde{\mu}_i(x,t)$ is the electrochemical potential. The electrical conductivity $\sigma_i(x,t)$ of charge carrier i is related to the diffusivity by the Nernst–Einstein relation

$$\sigma_i(x,t) = \frac{(z_i e)^2 D_i}{k_B T} c_i(x,t) \tag{2}$$

where D_i is the diffusivity (assumed independent of position and concentration), $c_i(x,t)$ is the carrier concentration, k_B is the Boltzmann constant and T is the absolute temperature. The electrochemical potential $\tilde{\mu}_i(x,t)$ is the sum of the chemical potential $\mu_i(x,t)$ and electrical energy $z_i e\phi(x,t)$

$$\tilde{\mu}_i(x,t) = \mu_i(x,t) + z_i e\phi(x,t) \tag{3}$$

where $\phi(x,t)$ is the electrical potential. The chemical potential $\mu_i(x,t)$ in the dilute limit is, in turn, given as

$$\mu_i(x,t) = \mu_i^0 + k_B T \ln\frac{c_i(x,t)}{c_i^0} \tag{4}$$

where μ_i^0 is the standard chemical potential, c_i^0 is the concentration of the total available lattice sites (where mobile electrons are taken to reside at cerium ion sites).

Eqn (1) can be rewritten in terms of charge flux and reduced potentials as

$$\begin{aligned} J_i^{\text{charge}}(x,t) &= -\frac{\sigma_i(x,t)}{z_i e}\frac{\partial \tilde{\mu}_i(x,t)}{\partial x} \\ &= -\sigma_i(x,t)\frac{\partial \tilde{\mu}_i^*(x,t)}{\partial x} \end{aligned} \tag{5}$$

with

$$J_i^{\text{charge}}(x,t) = z_i e J_i^{\text{mass}}(x,t) \tag{6}$$

$$\tilde{\mu}_i^*(x,t) = \frac{\tilde{\mu}_i(x,t)}{z_i e} = \mu_i^*(x,t) + \phi(x,t) \tag{7}$$

$$\mu_i^*(x,t) = \frac{\mu_i(x,t)}{z_i e} \tag{8}$$

where $J_i^{\text{charge}}(x,t)$ is the carrier charge flux, $\tilde{\mu}_i^*(x,t)$ is the reduced electrochemical potential and $\mu_i^*(x,t)$ is the reduced chemical potential. It is worth noting that both $\tilde{\mu}_i^*(x,t)$ and $\mu_i^*(x,t)$ have units of electrical potential. Inserting the expression for the chemical potential (4), the mass flux, eqn (1), becomes

$$\begin{aligned} J_i^{\text{mass}}(x,t) &= -D_i\frac{\partial c_i(x,t)}{\partial x} - \frac{\sigma_i(x,t)}{z_i e}\frac{\partial \phi(x,t)}{\partial x} \\ &= -D_i\frac{\partial c_i(x,t)}{\partial x} - \frac{z_i e D_i c_i(x,t)}{k_B T}\frac{\partial \phi(x,t)}{\partial x} \end{aligned} \tag{9}$$

and the charge flux, eqn (5), becomes

$$\begin{aligned} J_i^{\text{charge}}(x,t) &= -z_i e D_i\frac{\partial c_i(x,t)}{\partial x} - \sigma_i(x,t)\frac{\partial \phi(x,t)}{\partial x} \\ &= -z_i e D_i\frac{\partial c_i(x,t)}{\partial x} - \frac{(z_i e)^2 D_i c_i(x,t)}{k_B T}\frac{\partial \phi(x,t)}{\partial x} \end{aligned} \tag{10}$$

Eqns (9) and (10) have been given a variety of different names in the literature such as the diffusion-drift, diffusion-migration, Nernst–Planck or electrodiffusion equation.

The second fundamental equation is that describing continuity. In the case where there are no internal sources or sinks of mass, continuity requires that the variation in mass flux with position balances the variation in concentration with time according to

$$\frac{\partial c_i(x,t)}{\partial t} + \frac{\partial}{\partial x} J_i^{\text{mass}}(x,t) = 0 \tag{11}$$

In terms of charge flux, the continuity equation can be written as

$$z_i e \frac{\partial c_i(x,t)}{\partial t} + \frac{\partial}{\partial x} J_i^{\text{charge}}(x,t) = 0 \tag{12}$$

The third fundamental equation is that due to Poisson, which relates the sum of the charges in the system, $\sum_i z_i e c_i(x,t)$, to the electrical potential according to

$$-\varepsilon_r \varepsilon_0 \frac{\partial^2 \phi(x,t)}{\partial x^2} = \sum_i z_i e c_i(x,t) \tag{13}$$

where ε_r is the dielectric constant or relative permittivity, assumed to be time and position invariant, and ε_0 is the permittivity of free space (or vacuum).

Together, the continuity and Poisson equations imply the existence of a displacement flux. This is obtained as follows. As (12) is true for any species, it must also be true for the sum of all the species such that

$$\frac{\partial}{\partial t}\left[\sum_i z_i e c_i(x,t)\right] + \frac{\partial}{\partial x}\sum_i J_i^{\text{charge}}(x,t) = 0 \tag{14}$$

Insertion into eqn (13) yields

$$\frac{\partial}{\partial x}\left\{-\frac{\partial}{\partial t}\left[\varepsilon_r \varepsilon_0 \frac{\partial \phi(x,t)}{\partial x}\right]\right\} + \frac{\partial}{\partial x}\sum_i J_i^{\text{charge}}(x,t) = 0 \tag{15}$$

The integral of (15) with respect to position must thus be a constant (with respect to x), and this term can readily be recognized as the total charge flux:

$$J_{\text{T}}^{\text{charge}}(t) = J_{\text{dis}}^{\text{charge}}(x,t) + \sum_i J_i^{\text{charge}}(x,t) \tag{16}$$

where the displacement flux is

$$J_{\text{dis}}^{\text{charge}}(x,t) = -\frac{\partial}{\partial t}\left[\varepsilon_r \varepsilon_0 \frac{\partial \phi(x,t)}{\partial x}\right] \tag{17}$$

2.2 Boundary conditions: electrode properties

In order to solve the above system of equations to obtain such quantities as the concentration, the electric field, the chemical potential, and the flux, one requires, in principle, knowledge of the relevant boundary conditions. These can be formulated in terms of the fluxes at the electrolyte|electrode interfaces, quantities which are fixed by the values of the electrochemical potential at the respective interfaces and in the respective gas phase chambers. This type of boundary condition can be written in the most general case as

$$J_i^{\text{charge}}(0,t) = g[\tilde{\mu}_i^*(a,t), \tilde{\mu}_i^*(0,t)] \tag{18}$$

$$J_i^{\text{charge}}(L,t) = h[\tilde{\mu}_i^*(c,t), \tilde{\mu}_i^*(L,t)] \tag{19}$$

where $\tilde{\mu}_i^*(a,t)$ and $\tilde{\mu}_i^*(c,t)$ are the reduced electrochemical potentials at the electrodes a and c, g and h are functions which embody the characteristics of the electrochemical reactions. The boundary conditions for the displacement flux can be treated analogously.

The explicit forms of the boundary condition functions, g and h, depend on the details of the electrode reactions including steps such as adsorption, surface diffusion, charge transfer *etc*. Specification of the boundary conditions would further require complete knowledge of the relevant physical parameters such as surface coverage, surface diffusivity, charge transfer rate constants *etc*. In the absence of such detailed information, two typical expressions commonly encountered in the literature for the boundary functions are considered here. The first is the Butler–Volmer (B–V) equation, in which a portion of the voltage is taken to drive a concentration gradient and hence the overall rate of reaction.[16] Written in terms of the reduced electrochemical potential for the electrode a, the B–V equation is

$$J_i^{\text{charge}}(0,t) = J_{i0}(a)\left\{\exp\left[\alpha_i(a)\frac{e(\tilde{\mu}_i^*(a,t) - \tilde{\mu}_i^*(0,t))}{k_{\text{B}}T}\right] - \exp\left[-(1-\alpha_i(a))\frac{e(\tilde{\mu}_i^*(a,t) - \tilde{\mu}_i^*(0,t))}{k_{\text{B}}T}\right]\right\} \tag{20}$$

where $J_{i0}(a)$ is the exchange current density and $\alpha_i(a)$ is the transfer coefficient. When the arguments of the exponential terms are small, the B–V boundary condition can be approximated as a linear function

$$J_i^{\text{charge}}(0,t) = J_{i0}(a) e \frac{\tilde{\mu}_i^*(a,t) - \tilde{\mu}_i^*(0,t)}{k_{\text{B}}T} \tag{21}$$

The second common expression for g or h is the Chang–Jaffé (C–J) equation,[17] in which the overall rate of reaction is proportional to the voltage driving force

$$J_i^{\text{charge}}(0,t) = k_i(a)[\tilde{\mu}_i^*(a,t) - \tilde{\mu}_i^*(0,t)] \tag{22}$$

where $k_i(a)$ represents the rate constant of the electrochemical reaction.

If g and h are linear functions, as they are for the specific cases of eqns (21) and (22), then one can define a charge transfer resistance, $R_i^{\perp}(a)$, which relates the electrochemical potential drop at the interface to the flux across the interface:

$$\tilde{\mu}_i^*(a,t) - \tilde{\mu}_i^*(0,t) = J_i^{\text{charge}}(0,t) A R_i^{\perp}(a) \tag{23}$$

For the linearized B–V boundary condition, the charge transfer resistance is simply

$$R_i^{\perp}(a) = \frac{k_{\text{B}}T}{e J_{i0}(a) A} \tag{24}$$

whereas for the C–J boundary condition it is

$$R_i^{\perp}(a) = \frac{1}{k_i(a)A} \tag{25}$$

In addition to the specification of the electrochemical potential drop at the interface, a final set of boundary conditions is implied by the experimental conditions employed. That is, typically the total flux is given as an experimental input. In such a case, the solution to the coupled equations becomes relevant only to given experimental conditions. The two sets of conditions appropriate to the experiments performed here are discussed below.

2.3 Steady state solution under open circuit conditions

2.3.1 Transport through the MIEC. Under steady state conditions the system behavior is, by definition, independent of time. Explicitly removing the time dependence of the concentration profiles and of the fluxes from the continuity eqn (12) yields

$$\frac{\mathrm{d}}{\mathrm{d}x} J_i^{\mathrm{charge}}(x) = 0 \tag{26}$$

which thus implies that the charge flux is constant with position as well as time. The time independence of the generalized transport eqn (5) implies

$$J_i^{\mathrm{charge}} = -\sigma_i(x) \frac{\mathrm{d}\tilde{\mu}_i^*(x)}{\mathrm{d}x} \tag{27}$$

Similarly, the time independent form of the Poisson eqn (13) is

$$-\varepsilon_r \varepsilon_0 \frac{\mathrm{d}^2\phi(x)}{\mathrm{d}x^2} = \sum_i z_i e c_i(x) \tag{28}$$

The absence of a time dependence for the electric field, eqn (17), further implies that the displacement flux is zero. Thus, eqns (26)–(28) along with $J_{\mathrm{dis}}^{\mathrm{charge}}(x) = 0$, become the governing equations under steady state conditions. In the absence of an external applied electric potential gradient, *i.e.*, under open circuit conditions, the charge flux of all the carriers is balanced so as to produce no net charge flow. That is

$$J_{\mathrm{T}}^{\mathrm{charge}} = \sum_i J_i^{\mathrm{charge}} = 0 \tag{29}$$

which provides an additional constraint on the system.

It is of value to explicitly state the form of these relationships for the specific system under consideration here, acceptor doped ceria in which the three relevant species are oxygen ion vacancies, electrons and immobile acceptor dopants. Inserting the nature of the species into (27)–(29) yields

$$J_{\mathrm{ion}}^{\mathrm{charge}} = -\sigma_{\mathrm{ion}}(x) \frac{\mathrm{d}\tilde{\mu}_{\mathrm{ion}}^*(x)}{\mathrm{d}x} \tag{30}$$

$$J_{\mathrm{eon}}^{\mathrm{charge}} = -\sigma_{\mathrm{eon}}(x) \frac{\mathrm{d}\tilde{\mu}_{\mathrm{eon}}^*(x)}{\mathrm{d}x} \tag{31}$$

$$-\varepsilon_r \varepsilon_0 \frac{\mathrm{d}^2\phi(x)}{\mathrm{d}x^2} = 2e c_{\mathrm{ion}}(x) - e c_{\mathrm{eon}}(x) - e c_{A_D} \tag{32}$$

and

$$J_{\mathrm{ion}}^{\mathrm{charge}} + J_{\mathrm{eon}}^{\mathrm{charge}} = 0 \tag{33}$$

The above set of eqns (30)–(33), which completely describe the state of the system, are coupled, nonlinear, differential equations for which only numerical solutions are typically available. However, some approximate methods can be used to simplify the solution process. Two widely used approximations are the constant-field approximation and the electroneutrality approximation, both of which rely on the fact that the terms in eqn (32), and more generally in eqn (28), are small.[9,18] The *constant-field* approximation results when the left side term in eqn (28) is assumed to be zero, but the right side remains non-zero

$$-\varepsilon_r \varepsilon_0 \frac{\mathrm{d}^2\phi(x)}{\mathrm{d}x^2} = 0, \quad \sum_i z_i e c_i(x) \neq 0 \tag{34}$$

This implies

$$\frac{\mathrm{d}\phi(x)}{\mathrm{d}x} = -E \tag{35}$$

in which E is the electric field and is a constant. In the biological literature, this approach is usually called the Goldman constant field approximation.[19] The *electroneutrality* approximation results when the right-side term in eqn (28) is assumed to be zero, but the left side remains non-zero, the result is simply

$$\sum_i z_i e c_i(x) = 0, \quad -\varepsilon_r \varepsilon_0 \frac{\mathrm{d}^2\phi(x)}{\mathrm{d}x^2} \neq 0 \tag{36}$$

This is called the electroneutrality approximation since the total charge at any position is zero. This approximation has been employed in the work of Tannhauser[3] and of Liu.[6] There have been some investigation in the literature aimed at evaluating the validity of these approximations under various conditions.[18,20] The constant field approximation is more widely used because relatively simple analytical expressions can be obtained under certain conditions.

Another common approximation often employed is the so-called *constant vacancy approximation*. For a system such as that investigated here, in which the concentration of mobile ions (*i.e.*, oxygen vacancies) is essentially fixed by the constant dopant concentration, it is reasonable to approximate the mobile ion concentration as also being constant. Specifically, for acceptor doped ceria, the approximation becomes

$$c_{\mathrm{ion}} = c_{A_D}/2 \tag{37}$$

It is important to recognize that the constant field approximation is implicit in the constant oxygen vacancy approximation and this can be shown as follows. If the oxygen vacancy concentration is constant, then

$$\frac{\mathrm{d}c_{\mathrm{ion}}(x)}{\mathrm{d}x} = 0 \tag{38}$$

Combining this with the drift-diffusion eqn (10), and with the implication of a constant ionic conductivity as a result of the constant vacancy concentration one obtains

$$\frac{\mathrm{d}\phi(x)}{\mathrm{d}x} = -\frac{J_{\mathrm{ion}}^{\mathrm{charge}}}{\sigma_{\mathrm{ion}}} = -E \tag{39}$$

and thus the field is also a constant.

With these various approximations explicitly defined, it is possible to solve for the various unknown quantities in the system. Two basic approaches have been pursued in the solid state ionics literature, both within the context of the constant vacancy (and therefore constant field) approximation. The first is that of Riess,[4] most typically used to understand the electrical characteristics of mixed conductors and the second is that of Wagner,[2] most typically used to understand mass flux through such materials. The equivalence of these two approaches has been shown by Choudhury and Patterson[1] and by Yuan and Pal.[5] Here we base our analysis on the Riess[4] approach and explicitly extend it to a discussion of interfacial properties at the MIEC|electrode boundary.

In the approach developed by Riess,[4] the unknown concentration profiles are evaluated by taking the derivative of the flux (as given for the dilute limit approximation, eqn (9)) with respect to position

$$0 = -\frac{\mathrm{d}^2 c_i(x)}{\mathrm{d}x^2} - \frac{z_i e}{k_\mathrm{B}T}\frac{\mathrm{d}c_i(x)}{\mathrm{d}x}\frac{\mathrm{d}\phi(x)}{\mathrm{d}x} - \frac{z_i e}{k_\mathrm{B}T}c_i(x)\frac{\mathrm{d}^2\phi(x)}{\mathrm{d}x^2} \tag{40}$$

Under the constant field approximation, (35), this becomes

$$0 = \frac{\mathrm{d}^2 c_i(x)}{\mathrm{d}x^2} - \frac{z_i eE}{k_\mathrm{B}T}\frac{\mathrm{d}c_i(x)}{\mathrm{d}x} \tag{41}$$

Taking eqn (41) to apply to the electron concentration (and not vacancies which are instead described by the constant vacancy approximation), the solution for $c_{\mathrm{eon}}(x)$ is

$$c_{\mathrm{eon}}(x) = c_{\mathrm{eon}}(0) - [c_{\mathrm{eon}}(0) - c_{\mathrm{eon}}(L)] \times \frac{1-\exp\left(-\frac{eE}{k_\mathrm{B}T}x\right)}{1-\exp\left(-\frac{eE}{k_\mathrm{B}T}L\right)} \tag{42}$$

which also implies

$$\sigma_{\mathrm{eon}}(x) = \sigma_{\mathrm{eon}}(0) - [\sigma_{\mathrm{eon}}(0) - \sigma_{\mathrm{eon}}(L)] \times \frac{1-\exp\left(-\frac{eE}{k_\mathrm{B}T}x\right)}{1-\exp\left(-\frac{eE}{k_\mathrm{B}T}L\right)} \tag{43}$$

Inserting the electron concentration and conductivity profiles of eqns (42) and (43) into the drift-diffusion equation, eqn (10), and again making use of the constant field approximation, (35), yields the electron flux:

$$J_{\mathrm{eon}}^{\mathrm{charge}} = \frac{\sigma_{\mathrm{eon}}(L) - \sigma_{\mathrm{eon}}(0)\exp\left(-\frac{eE}{k_\mathrm{B}T}L\right)}{1-\exp\left(-\frac{eE}{k_\mathrm{B}T}L\right)}E \tag{44}$$

Using the fact that the electron and ionic charge fluxes are exactly balanced under steady state conditions, eqn (33), and combining this with the solution to the electric field under the constant vacancy approximation, eqn (39), one obtains the electric field, necessary for the evaluation of eqns (42)–(44).

$$E = -\frac{k_\mathrm{B}T}{eL}\ln\frac{\sigma_{\mathrm{ion}} + \sigma_{\mathrm{eon}}(L)}{\sigma_{\mathrm{ion}} + \sigma_{\mathrm{eon}}(0)} = \frac{\phi(L) - \phi(0)}{L} \tag{45}$$

The ionic charge flux can then be evaluated either from $J_{\mathrm{ion}}^{\mathrm{charge}} = -J_{\mathrm{ion}}^{\mathrm{charge}}$, with the latter as given in (44), or from

$$J_{\mathrm{ion}}^{\mathrm{charge}} = \sigma_{\mathrm{ion}}E = -\frac{k_\mathrm{B}T\sigma_{\mathrm{ion}}}{eL}\ln\frac{\sigma_{\mathrm{ion}} + \sigma_{\mathrm{eon}}(L)}{\sigma_{\mathrm{ion}} + \sigma_{\mathrm{eon}}(0)} \tag{46}$$

The *voltage* across the mixed conducting electrolyte is given not directly by the electric field, but is rather determined by the difference in reduced electrochemical potential of the electronic species

$$V(L) - V(0) = \tilde{\mu}^*_{\mathrm{eon}}(L) - \tilde{\mu}^*_{\mathrm{eon}}(0) \tag{47}$$

Rewriting (47) in terms of the chemical and electrical potentials, eqns (7) and (8), and making use of the dilute limit approximation for the chemical potential of electrons, eqn (4), gives

$$V(L) - V(0) = \frac{k_\mathrm{B}T}{-e}\ln\frac{c_{\mathrm{eon}}(L)}{c_{\mathrm{eon}}(0)} + \phi(L) - \phi(0) \tag{48}$$

Inserting the value of the electric field, eqn (45), into the above then yields

$$V(L) - V(0) = -\frac{k_\mathrm{B}T}{e}\ln\frac{c_{\mathrm{eon}}(L)}{c_{\mathrm{eon}}(0)} + \frac{k_\mathrm{B}T}{e}\ln\frac{\sigma_{\mathrm{ion}} + \sigma_{\mathrm{eon}}(L)}{\sigma_{\mathrm{ion}} + \sigma_{\mathrm{eon}}(0)} \tag{49}$$

for the voltage. Thus, under the constant vacancy approximation, one need only know the value of the material properties at the electrolyte|electrode interfaces (*i.e.*, at $x = 0$ and $x = L$) and one can immediately evaluate the charge fluxes and the electronic conductivity and concentration profiles.

If one wishes to extract a virtual oxygen potential profile based on the constant vacancy approach, one requires a relationship between electron concentration and oxygen partial pressure. This can be achieved by assuming local equilibrium for the reaction

$$\mathrm{O}_\mathrm{O}^\times \leftrightarrow \frac{1}{2}\mathrm{O}_2 + V_\mathrm{O}^{\bullet\bullet} + 2e' \tag{50}$$

where $O_\mathrm{o}^\times$ represents, in the Kröger–Vink notation, oxygen residing on a regular oxygen site. Under this assumption, the electrochemical potentials of the relevant species are related according to

$$\frac{1}{2}\mu_{\mathrm{O}_2}(x) + \tilde{\mu}_{\mathrm{ion}}(x) + 2\tilde{\mu}_{\mathrm{eon}}(x) = 0 \tag{51}$$

(where $\tilde{\mu}_{\mathrm{O}_2}(x) = \mu_{\mathrm{O}_2}(x)$), or, in terms of reduced electrochemical potential for the charged species, according to

$$\frac{1}{4e}\mu_{\mathrm{O}_2}(x) + \tilde{\mu}^*_{\mathrm{ion}}(x) - \tilde{\mu}^*_{\mathrm{eon}}(x) = 0 \tag{52}$$

Taking oxygen to behave as an ideal gas, its chemical potential is

$$\mu_{\mathrm{O}_2} = \mu^0_{\mathrm{O}_2} + k_\mathrm{B}T\ln p_{\mathrm{O}_2} \tag{53}$$

and the equilibrium reaction constant, K_r, for eqn (51) becomes

$$K_r = c_{\mathrm{ion}}(x)c^2_{\mathrm{eon}}(x)p^{1/2}_{\mathrm{O}_2}(x) \tag{54}$$

The oxygen partial pressure profile is then simply

$$p_{O_2}(x) = \left[\frac{K_r}{c_{ion} c_{eon}^2(x)}\right]^2 \tag{55}$$

where the electron concentration can be evaluated according to eqn (42), and the vacancy concentration is now explicitly indicated as position independent.

The local equilibrium approximation further allows one to express the voltage and the flux across the mixed conductor in terms of the oxygen partial pressures at the electrode|electrolyte interfaces. Specifically, the electron conductivity profile becomes

$$\sigma_{eon}(x) = \frac{D_{eon} e^2}{k_B T} c_{eon}(x) = \sigma_{eon}^0 \, p_{O_2}^{-1/4}(x) \tag{56}$$

with

$$\sigma_{eon}^0 = \frac{D_{eon} e^2}{k_B T} \left(\frac{K_r}{c_{ion}}\right)^{1/2} \tag{57}$$

Upon insertion of (56) and the oxygen partial pressure dependence of $c_{eon}(x)$ implied by (55) into (49), the voltage becomes

$$\begin{aligned} V(L) - V(0) =& \tilde{\mu}_{eon}^*(L) - \tilde{\mu}_{eon}^*(0) \\ =& \frac{k_B T}{e} \ln \frac{\sigma_{eon}^0 + \sigma_{ion} \, p_{O_2}^{1/4}(L)}{\sigma_{eon}^0 + \sigma_{ion} \, p_{O_2}^{1/4}(0)} \end{aligned} \tag{58}$$

Similarly, insertion of (56) into the flux expression of (46) yields

$$J_{ion}^{charge} = -\frac{k_B T \sigma_{ion}}{eL} \ln \frac{\sigma_{ion} + \sigma_{eon}^0 \, p_{O_2}^{-1/4}(L)}{\sigma_{ion} + \sigma_{eon}^0 \, p_{O_2}^{-1/4}(0)} \tag{59}$$

These expressions emphasize the significance of knowledge of the oxygen partial pressure at the electrode|electrolyte interfaces, rather than merely within the electrode chambers, in order to describe the various characteristics of the system.

As already indicated, many of these relationships have been previously presented in the literature. They are summarized here for completeness and because they serve as a starting point for understanding the influence of electrode behavior and for evaluating charge transport under a broader set of experimental conditions.

2.3.2 Electrode behavior: application of boundary conditions. A complete description of the electrode|MIEC|electrode system requires application of the boundary conditions discussed in section 2.2. While the flux through the system is a constant under steady state conditions, the voltage will be influenced by the electrochemical activity of the electrodes. The macroscopically measured voltage generated between the anode and cathode electrodes, corresponding to the open circuit voltage (OCV or V_{oc}), is given as

$$V_{oc} = V(c) - V(a) = \tilde{\mu}_{eon}^*(c) - \tilde{\mu}_{eon}^*(a) \tag{60}$$

Under the assumption of local chemical equilibrium for reaction (50), the electrochemical potentials of the species in the electrodes chambers are related according to

$$\frac{1}{4e}\mu_{O_2}(a) + \tilde{\mu}_{ion}^*(a) - \tilde{\mu}_{eon}^*(a) = 0 \tag{61}$$

$$\frac{1}{4e}\mu_{O_2}(c) + \tilde{\mu}_{ion}^*(c) - \tilde{\mu}_{eon}^*(c) = 0 \tag{62}$$

Inserting the expressions implied by these relationships for $\tilde{\mu}_{ion}^*(c)$ and $\tilde{\mu}_{ion}^*(a)$ into (60) yields

$$V_{oc} = \frac{1}{4e}\mu_{O_2}(c) - \frac{1}{4e}\mu_{O_2}(a) + \tilde{\mu}_{ion}^*(c) - \tilde{\mu}_{ion}^*(a) \tag{63}$$

The difference between the first two terms in (63) is readily recognized as the Nernst potential, V_N, of the system

$$V_N = \frac{1}{4e}[\mu_{O_2}(c) - \mu_{O_2}(a)] = \frac{k_B T}{4e} \ln \frac{p_{O_2}(c)}{p_{O_2}(a)} \tag{64}$$

The final two terms in (63) can be evaluated by reference to the charge transfer resistance, as defined in (23). That definition implies

$$\tilde{\mu}_{ion}^*(a) - \tilde{\mu}_{ion}^*(0) = J_{ion}^{charge} A R_{ion}^{\perp}(a) \tag{65}$$

$$\tilde{\mu}_{ion}^*(L) - \tilde{\mu}_{ion}^*(c) = J_{ion}^{charge} A R_{ion}^{\perp}(c) \tag{66}$$

and thus (63) becomes

$$V_{oc} = V_N + \tilde{\mu}_{ion}^*(L) - \tilde{\mu}_{ion}^*(0) - J_{ion}^{charge} A [R_{ion}^{\perp}(a) + R_{ion}^{\perp}(c)] \tag{67}$$

The quantity $\tilde{\mu}_{ion}^*(L) - \tilde{\mu}_{ion}^*(0)$ in this expression can be obtained by integration of (30) and is given as

$$\tilde{\mu}_{ion}^*(L) - \tilde{\mu}_{ion}^*(0) = -J_{ion}^{charge} A R_{ion} \tag{68}$$

with

$$R_{ion} = \int_0^L \frac{dx}{\sigma_{ion} A} \tag{69}$$

where R_{ion} is defined as the total ionic resistance of the electrolyte. Thus, the externally measured voltage or OCV is

$$V_{oc} = V_N - J_{ion}^{charge} A [R_{ion}^{\perp}(a) + R_{ion} + R_{ion}^{\perp}(c)] \tag{70}$$

This voltage depends not only on the oxygen partial pressures at the electrodes (which establish V_N), but also on the ionic resistivity of the electrolyte and the electrochemical activity of the electrodes.

The voltage can also be alternatively expressed in terms of the electronic properties of the MIEC, if again, appropriate boundary conditions are applied. If the electrodes are taken to be reversible with respect to electrons, such that the variation in electrochemical potential of electrons throughout each electrode and across each electrode|electrolyte interface is assumed to be negligible, then

$$\tilde{\mu}_{eon}^*(a) = \tilde{\mu}_{eon}^*(0) \tag{71}$$

$$\tilde{\mu}_{eon}^*(c) = \tilde{\mu}_{eon}^*(L) \tag{72}$$

Insertion into (60) simply yields

$$V_{oc} = \tilde{\mu}_{eon}^*(L) - \tilde{\mu}_{eon}^*(0) \tag{73}$$

which can be evaluated by integration of (31) to obtain

$$\tilde{\mu}^*_{\text{eon}}(L) - \tilde{\mu}^*_{\text{eon}}(0) = -J^{\text{charge}}_{\text{eon}} A R_{\text{eon}} = V_{\text{oc}} \tag{74}$$

with

$$R_{\text{eon}} = \int_0^L \frac{\mathrm{d}x}{\sigma_{\text{eon}}(x) A} \tag{75}$$

where $\underline{R}_{\text{eon}}$ is defined as the total electronic resistance of the electrolyte. The assumption of electron-reversible electrodes moreover implies that the voltage across the mixed conductor, as expressed in (58) becomes identical to the measured OCV, *i.e.*,

$$V_{\text{oc}} = \frac{k_{\text{B}}T}{e} \ln \frac{\sigma^0_{\text{eon}} + \sigma_{\text{ion}}\, p^{1/4}_{\text{O}_2}(L)}{\sigma^0_{\text{eon}} + \sigma_{\text{ion}}\, p^{1/4}_{\text{O}_2}(0)} \tag{76}$$

This treatment takes the voltage drop across the electrode|electrolyte interfaces to be zero (implied in the statement that there is no change in the electrochemical potential of the electrons across these interfaces). However, there is a change in oxygen chemical potential (and hence also a change in virtual oxygen partial pressure) across the electrodes and/or across the interface as a consequence of non-ideal kinetics for the electrochemical reactions. The situation is shown schematically in Fig. 2. For simplicity, the oxygen chemical potential and the oxygen ion electrochemical potential are taken to be single-valued at the electrode|electrolyte interface, but such a situation is not required, and these properties may, in principle, be discontinuous at the interface. By influencing the potentials at the surfaces of the electrolyte, the characteristics of the electrodes influence the electrochemical behavior of the MIEC. Specifically, the electrodes establish the oxygen partial pressures at $x = 0$ and L, which, in turn, set the total electronic conductivity of the MIEC by fixing the values of the electronic conductivity at the integration limits of (75). The change in partial pressure across the electrodes and across the electrode|electrolyte interfaces, furthermore, contributes, along with the electronic leakage, to the reduction of the cell voltage below the Nernstian value.

Physically, the oxygen chemical potential change across the electrodes must be related to the atomistic terms describing the

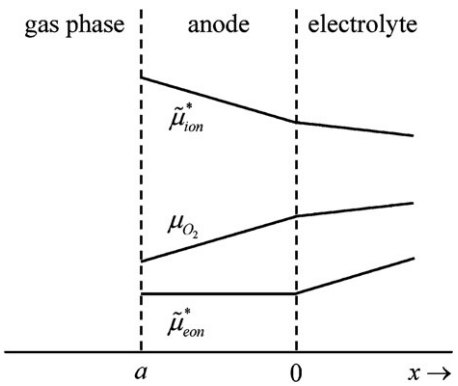

Fig. 2 Schematic illustration of the chemical potential changes occurring at an electrode|electrolyte interface, shown for the particular case of the anode, under the assumption of an electron reversible electrode.

boundary conditions. The electron reversibility of the electrodes implies from (61)

$$\frac{1}{4e}\mu_{\text{O}_2}(a) + \tilde{\mu}^*_{\text{ion}}(a) - \tilde{\mu}^*_{\text{eon}}(0) = 0 \tag{77}$$

Simultaneously, the local chemical equilibrium at the anode|electrolyte interface implies

$$\frac{1}{4e}\mu_{\text{O}_2}(0) + \tilde{\mu}^*_{\text{ion}}(0) - \tilde{\mu}^*_{\text{eon}}(0) = 0 \tag{78}$$

Taking the difference yields

$$\frac{1}{4e}(\mu_{\text{O}_2}(a) - \mu_{\text{O}_2}(0)) + \tilde{\mu}^*_{\text{ion}}(a) - \tilde{\mu}^*_{\text{ion}}(0) = 0 \tag{79}$$

Defining $\Delta\mu_{\text{O}_2}(a,0)$ as the difference between the oxygen chemical potential in the anode gas chamber and that at the electrolyte interface, and making use of (65) gives

$$\Delta\mu_{\text{O}_2}(a,0) = -4eJ^{\text{charge}}_{\text{ion}} A R^{\perp}_{\text{ion}}(a) \tag{80}$$

Inserting the expressions for the charge transfer resistance obtained from the B–V and the C–J boundary conditions, (24) and (25), respectively, yields

$$\Delta\mu_{\text{O}_2}(a,0) = -4k_{\text{B}}T \frac{J^{\text{charge}}_{\text{ion}}}{J_{\text{ion},0}(a)} \tag{81}$$

and

$$\Delta\mu_{\text{O}_2}(a,0) = \frac{-4e}{k_{\text{ion}}(a)} J^{\text{charge}}_{\text{ion}} \tag{82}$$

These relationships yield the expected result that, in the limit of infinitely large exchange current density or infinitely large reaction rate, the change in oxygen chemical potential across the electrodes is zero.

For ease of interpretation, eqns (70) and (74) can be mapped to an equivalent DC circuit, specifically, to that shown in Fig. 3. Here, an electronic path (or rail) lies in parallel with an ionic path (or rail), where the latter includes resistors representative of the electrode characteristics and also the Nernstian voltage source. A flux $J^{\text{charge}}_{\text{eon}}$ flows through resistor R_{eon}, and the voltage across this resistor, which corresponds to that measured at open circuit, is that expressed in (74). Similarly, a flux $J^{\text{charge}}_{\text{ion}}$ (of identical magnitude but opposite sign to $J^{\text{charge}}_{\text{eon}}$) flows through resistors $R^{\perp}_{\text{ion}}(a)$, R_{ion}, and $R^{\perp}_{\text{ion}}(c)$. The sum of the voltage drops across these three resistors together with the Nernstian voltage source corresponds to expression (70) for the open circuit voltage. Depending on the nature of the boundary conditions, the resistors $R^{\perp}_{\text{ion}}(a)$ and $R^{\perp}_{\text{ion}}(c)$ can be replaced by nonlinear components while retaining the simplicity of the depicted equivalent circuit. Although the mapping produces the desired mathematical result, it is emphasized that there is no physical voltage drop across the electrodes under the assumption of electron reversible electrodes. The electrode ''resistors'' account for the oxygen partial pressure drop across the electrodes which generate effective voltage drops.

Given the relationship between $J^{\text{charge}}_{\text{eon}}$ and $J^{\text{charge}}_{\text{ion}}$, (33), the measured open circuit voltage can be expressed as

$$V_{\text{oc}} = \frac{R_{\text{eon}}}{R_{\text{eon}} + R^{\perp}_{\text{ion}}(a) + R_{\text{ion}} + R^{\perp}_{\text{ion}}(c)} V_{\text{N}} \tag{83}$$

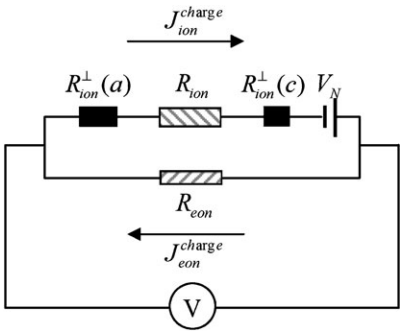

Fig. 3 DC equivalent circuit of a mixed conductor under open circuit conditions. Ion transfer across the electrode|electrolyte interface is assumed to display Chang–Jaffé or linearized Butler–Volmer behavior, whereas electron transfer is assumed to be reversible.

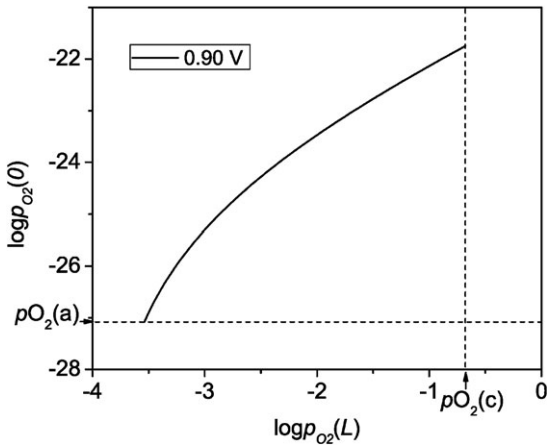

Fig. 4 Correlation between $p_{O_2}(0)$ and $p_{O_2}(L)$ according to equation assuming an experimental value for V_{oc} across SDC15 of 0.90 V at conditions T = 600 °C, $p_{O_2}(c)$ = 0.21 atm and $p_{O_2}(a)$ = 8.3 × 10^{-28} atm. The oxygen partial pressure at the anode|electrolyte interface must fall within the range 8.3 × 10^{-18} and 1.8 × 10^{-22} atm, and that at the cathode|electrolyte interface within the range 2.9 × 10^{-4} and 0.21 atm.

a result that can be obtained from direct evaluation of the circuit of Fig. 3 or by combining (70), (74) and (33). The effective contribution of the electrodes to the loss in open circuit potential is immediately evident in this formulation. In the case of ideally active electrodes with $R_{ion}^{\perp}(a)$, $R_{ion}^{\perp}(c) \rightarrow 0$, the oxygen partial pressures at the $x = 0$ and $x = L$ match precisely the respective values in the anode and cathode chambers (see eqn (80)), and the theoretical maximum voltage across the mixed conductor, V_{oc}^{th}, is obtained, where

$$V_{oc}^{th} = \frac{R_{eon}}{R_{eon} + R_{ion}} V_N = \frac{R_{eon}}{R_{eon} + R_{ion}} \frac{k_B T}{4e} \ln \frac{p_{O_2}(c)}{p_{O_2}(a)} \quad (84)$$

By making use of (58) and the equality of the oxygen partial pressures at the interfaces to those values in the electrode chambers, this can alternatively be expressed as

$$V_{oc}^{th} = \frac{k_B T}{e} \ln \frac{\sigma_{eon}^0 + \sigma_{ion}\, p_{O_2}^{1/4}(c)}{\sigma_{eon}^0 + \sigma_{ion}\, p_{O_2}^{1/4}(a)} \quad (85)$$

A noteworthy consequence of these relationships is that it is not possible to directly evaluate the mean ionic transference number of a mixed conductor from a simple measurement of the voltage at open circuit unless care is taken to develop ion reversible electrodes (which is not the case for the typical experiment). That is, in general, $\langle t_{ion} \rangle \neq V_{oc}/V_N$, a result which has received some attention in the recent literature.[21]

In light of the ambiguity inherent in (83), it is of value to consider what one can, in fact, establish from a measurement of the OCV. As expressed in (76), V_{oc} contains two unknown parameters, $p_{O_2}(0)$ and $p_{O_2}(L)$. If one has some basis for specifying the value of one of these terms (perhaps using a reference electrode or from independent studies of one of the electrode materials), and one additionally has knowledge of σ_{eon}^0 and σ_{ion}, then the oxygen partial pressure at the other interface can be specified. An example of the correlation between the two interfacial partial pressures in SDC15 is plotted in Fig. 4, where the bulk material properties are taken from ref. 14 the experimental conditions are taken to be $p_{O_2}(c)$ = 0.21 atm, $p_{O_2}(a)$ = 8.3 × 10^{-28} atm and temperature = 600 °C, and the "experimental" OCV is taken to be 0.90 V. Under these conditions, the Nernst voltage is 1.208 V and the theoretical OCV for ideal electrodes, calculated according to (85), is 1.025 V. For a given measured voltage, an increasing cathode activity, as reflected by high $p_{O_2}(L)$, implies a low anode activity, as reflected by high $p_{O_2}(0)$. Most significantly, the experimentally measured voltage, although it cannot alone yield the values of $p_{O_2}(0)$ and $p_{O_2}(L)$, places a lower boundary on the activities of the individual electrodes. For the example illustrated here, the activity of the cathode must be such that $p_{O_2}(L)$ is at least 2.9 × 10^{-4} atm and that of the anode must be such that $p_{O_2}(0)$ is less than 1.8 × 10^{-22} atm.

2.4 Small signal impedance solution under open circuit conditions

2.4.1 Transport through the MIEC. With the steady state solution in hand, it is possible to consider the situation upon application of a small perturbation. Such a perturbation, which could be a sinusoidal signal, a square-wave signal or other periodic or aperiodic form, causes the system to evolve with time. For a sufficiently small perturbation, all quantities can be written as the sum of their steady state values and the time dependent perturbations to those values

$$\begin{aligned}
\phi(x,t) &= \phi(x) + \Delta\phi(x,t) \\
c_i(x,t) &= c_i(x) + \Delta c_i(x,t) \\
\sigma_i(x,t) &= \sigma_i(x) + \Delta\sigma_i(x,t) \\
\tilde{\mu}_i^*(x,t) &= \tilde{\mu}_i^*(x) + \Delta\tilde{\mu}_i^*(x,t) \\
J_i^{charge}(x,t) &= J_i^{charge} + \Delta J_i^{charge}(x,t) \\
J_{dis}^{charge}(x,t) &= \Delta J_{dis}^{charge}(x,t) \\
J_T^{charge}(t) &= \Delta J_T^{charge}(t)
\end{aligned} \quad (86)$$

Insertion of (86) and the steady state expression (27) into the generalized flux eqn (5) and the continuity eqn (12) then yields

$$\Delta J_i^{\text{charge}}(x,t) = -\sigma_i(x)\frac{\partial \Delta\tilde{\mu}_i^*(x,t)}{\partial x} - \Delta\sigma_i(x,t)\frac{\mathrm{d}\tilde{\mu}_i^*(x)}{\mathrm{d}x} \quad (87)$$

$$-\frac{\partial \Delta J_i^{\text{charge}}(x,t)}{\partial x} = z_i e\frac{\partial \Delta c_i(x,t)}{\partial t} \quad (88)$$

where the second order term $\Delta\sigma_i(x,t)\frac{\partial}{\partial x}\Delta\tilde{\mu}_i^*(x,t)$ has been ignored. Further evaluation of these relationships is made possible by converting the terms in $\Delta\sigma$ and Δc into terms in $\Delta\tilde{\mu}^*$ and $\Delta\mu^*$. This is achieved as follows. In the dilute limit, (4), perturbations in concentration are related to perturbations in chemical potential according to

$$\begin{aligned}\Delta c_i(x,t) =& c_i(x)\left[\frac{c_i(x,t)}{c_i(x)} - 1\right] \\ =& c_i(x)\left\{\exp\left[\frac{\Delta\mu_i(x,t)}{k_{\text{B}}T}\right] - 1\right\}\end{aligned} \quad (89)$$

For small values for the argument of the exponent (*i.e.* a small perturbation), the second order term $\Delta\mu_i(x,t)\Delta\mu_i(x,t)$ can be ignored and the exponential term can be approximated as

$$\exp\left[\frac{\Delta\mu_i(x,t)}{k_{\text{B}}T}\right] \approx 1 + \frac{\Delta\mu_i(x,t)}{k_{\text{B}}T} \quad (90)$$

Thus (89) becomes

$$\Delta c_i(x,t) = c_i(x)\frac{\Delta\mu_i(x,t)}{k_{\text{B}}T} = z_i e c_i(x)\frac{\Delta\mu_i^*(x,t)}{k_{\text{B}}T} \quad (91)$$

and (88) can be rewritten as

$$-\frac{\partial \Delta J_i^{\text{charge}}(x,t)}{\partial x} = \frac{(z_i e)^2 c_i(x)}{k_{\text{B}}T}\,\frac{\partial \Delta\mu_i^*(x,t)}{\partial t} \quad (92)$$

The perturbation in conductivity can, *via* the Nernst–Einstein relationship, (2), and the result in (91), also be written in terms of the perturbation in chemical potential

$$\Delta\sigma_i(x,t) = \sigma_i(x)\frac{\Delta\mu_i(x,t)}{k_{\text{B}}T} \quad (93)$$

Along with (27) this allows (87) to be rewritten as

$$\begin{aligned}\Delta J_i^{\text{charge}}(x,t) =& -\sigma_i(x)\frac{\partial \Delta\tilde{\mu}_i^*(x,t)}{\partial x} \\ &+ z_i e J_i^{\text{charge}}\frac{\Delta\mu_i^*(x,t)}{k_{\text{B}}T}\end{aligned} \quad (94)$$

The perturbation in the total charge flux, $\Delta J_{\text{T}}^{\text{charge}}$, and the displacement flux, $\Delta J_{\text{T}}^{\text{charge}}(x,t)$, are readily obtained by direct insertion of (86) into (16) and (17), respectively, giving

$$\Delta J_{\text{T}}^{\text{charge}}(t) = \sum_i \Delta J_i^{\text{charge}}(x,t) + \Delta J_{\text{dis}}^{\text{charge}}(x,t) \quad (95)$$

and

$$\Delta J_{\text{dis}}^{\text{charge}}(x,t) = -\varepsilon_r\varepsilon_0\frac{\partial}{\partial x}\frac{\partial}{\partial t}\Delta\phi(x,t) \quad (96)$$

Experimentally, it is typical to apply a sinusoidal perturbation to a materials system. Hence, it is convenient to transform the above relationships from the time to the frequency domain. The Laplace transforms, respectively, of (94), (92), (96), and (95) are

$$\begin{aligned}\Delta J_i^{\text{charge}}(x,\omega) =& -\sigma_i(x)\frac{\partial \Delta\tilde{\mu}_i^*(x,\omega)}{\partial x} \\ &+ \frac{z_i e J_i^{\text{charge}}}{k_{\text{B}}T}\Delta\mu_i^*(x,\omega)\end{aligned} \quad (97)$$

$$\frac{\partial \Delta J_i^{\text{charge}}(x,\omega)}{\partial x} = -j\omega\frac{(z_i e)^2 c_i(x)}{k_{\text{B}}T}\Delta\mu_i^*(x,\omega) \quad (98)$$

$$\Delta J_{\text{dis}}^{\text{charge}}(x,\omega) = -j\omega\varepsilon_r\varepsilon_0\frac{\partial \Delta\phi(x,\omega)}{\partial x} \quad (99)$$

$$\Delta J_{\text{T}}^{\text{charge}}(\omega) = \Delta J_{\text{dis}}^{\text{charge}}(x,\omega) + \sum_i \Delta J_i^{\text{charge}}(x,\omega) \quad (100)$$

where $j = \sqrt{-1}$ and ω is angular frequency.

In analogy to previous studies of the electrical properties of a mixed conductor under uniform chemical conditions,[22] solutions to this new set of coupled differential equations can be approached by discretization. This is achieved by replacing the continuous position variable x with a set of discrete grid points, x_i, Fig. 5. In principle, these points may be separated from one another by differing distances, as illustrated in the figure, but for the computations performed here the distance between grid points was fixed to a constant value, l. The total number of grid points is $N + 1$ with $x_0 = 0$ and $x_N = L$, and each differential unit is taken to extend between the midpoints of neighboring grid points, as shown in Fig. 5. After establishing the grid system, the system of volume elements is constructed by assigning the entire structure and thus each of the differential units cross-sectional area A. Evaluation of the flux terms at the edges of the volume elements (between grid mid-points) and the remaining functions, $\Delta\phi_i$, $\Delta\tilde{\mu}_i^*$,

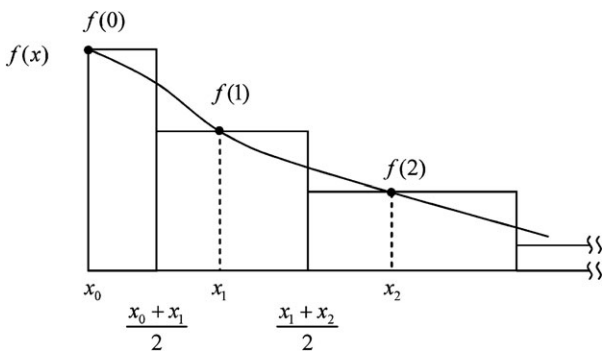

Fig. 5 The system of grid discretization and volume elements used in the numerical solution of the transport equations. Grid points correspond to x_n positions and the volume elements extend between the midpoints of neighboring gridpoints, *i.e.* between $\left(\frac{x_n+x_{n+1}}{2}\right)$ points.

and $\Delta\mu_i^*$, c_i and σ_i, directly at the grid points transforms eqns (97)–(99) into

$$\Delta J_i^{\text{charge}}(\bar{x}_n,\omega) = -\overline{\sigma_i(x_n)}\frac{\Delta\tilde{\mu}_i^*(x_{n+1},\omega)-\Delta\tilde{\mu}_i^*(x_n,\omega)}{x_{n+1}-x_n} + \frac{z_i e J_i^{\text{charge}}}{k_{\text{B}}T}\frac{\Delta\mu_i^*(x_{n+1},\omega)+\Delta\mu_i^*(x_n,\omega)}{2}; \quad .....0 \le n \le N-1 \tag{101}$$

$$\Delta J_i^{\text{charge}}(\bar{x}_n,\omega) - \Delta J_i^{\text{charge}}(\bar{x}_{n-1},\omega) = -j\omega\frac{(z_i e)^2 c_i(x_n)}{k_B T}\frac{x_{n+1}-x_{n-1}}{2}\Delta\mu_i^*(x_n,\omega); \quad ...1 \le n \le N-1 \tag{102}$$

$$\Delta J_{\text{dis}}^{\text{charge}}(\bar{x}_n,\omega) = -j\omega\varepsilon_r\varepsilon_0\frac{\Delta\phi(x_{n+1},\omega)-\Delta\phi(x_n,\omega)}{x_{n+1}-x_n}; \quad .....0 \le n \le N-1 \tag{103}$$

where

$$\bar{x}_n = \frac{x_n + x_{n+1}}{2}$$

$$\overline{\sigma(x_n)} = \frac{\sigma(x_n)+\sigma(x_{n+1})}{2}$$

Expression (100) states that the perturbation in total charge flux is independent of position and therefore of the grid point at which it is evaluated. This observation allows one to write

$$\Delta J_{\text{dis}}^{\text{charge}}(\bar{x}_{n-1},\omega) + \sum_i \Delta J_i^{\text{charge}}(\bar{x}_{n-1},\omega) = \Delta J_{\text{dis}}^{\text{charge}}(\bar{x}_n,\omega) + \sum_i \Delta J_i^{\text{charge}}(\bar{x}_n,\omega); .....1 \le n \le N-1 \tag{104}$$

completing the transformation to discretized relationships.

Physical insight into the significance of above set of transport eqns (101)–(104) can be gained by expressing them in the general form $I = V/Z$, where I is current, V is voltage and Z is electrical impedance, which ultimately allows the equations to be mapped to electrical circuit elements. Specifically, upon multiplication by the area, A, the ΔJ^{charge} terms can be replaced by electrical current I terms; the driving force terms $\Delta\phi_i$, $\Delta\tilde{\mu}_i^*$, and $\Delta\mu_i^*$ can be replaced by voltage terms; and the material properties can be collected into impedance terms. The result is

$$I_i(n) = -\frac{V_i(n+1)-V_i(n)}{Z_i(n)} + \frac{V_i(n+1)-V_{\text{dis}}(n+1)}{Z_i^0} + \frac{V_i(n)-V_{\text{dis}}(n)}{Z_i^0}$$
$$= -\frac{V_i(n+1)-V_i(n)}{Z_i(n)} + I_i^0(n+1) + I_i^0 .....0 \le n \le N-1 \tag{105}$$

$$I_i(n) - I_i(n-1) = -\frac{V_i(n)-V_{\text{dis}}(n)}{Z_i^{\text{chem}}(n)}; .....1 \le n \le N-1 \tag{106}$$

$$I_{\text{dis}}(n) = -\frac{V_{\text{dis}}(n+1)-V_{\text{dis}}(n)}{Z_{\text{dis}}(n)}; .....0 \le n \le N-1 \tag{107}$$

$$I_{\text{dis}}(n-1) + \sum_i I_i(n-1) = I_{\text{dis}}(n) + \sum_i I_i(n); .....1 \le n \le N-1 \tag{108}$$

where

$$Z_i(n) = R_i(n) = \left[\overline{\sigma(x_n)}\right]^{-1}\frac{x_{n+1}-x_n}{A} = \frac{l}{\overline{\sigma(x_n)}A}; .....0 \le n \le N-1$$

$$Z_{\text{dis}}(n) = [j\omega C_{\text{dis}}(n)]^{-1}; .....0 \le n \le N-1$$

$$C_{\text{dis}}(n) = \varepsilon_r\varepsilon_0\frac{A}{x_{n+1}-x_n} = \varepsilon_r\varepsilon_0\frac{A}{l}; .....0 \le n \le N-1$$

$$Z_i^{\text{chem}}(n) = [j\omega C_i^{\text{chem}}(n)]^{-1}; .....1 \le n \le N-1$$

$$C_i^{\text{chem}}(n) = \frac{(z_i e)^2 c_i(x_n)}{k_{\text{B}}T}\frac{x_{n+1}-x_{n-1}}{2}A = \frac{(z_i e)^2 c_i(x_n)}{k_{\text{B}}T}lA; .....1 \le n \le N-1$$

$$Z_i^0 = R_i^0 = \frac{2k_{\text{B}}T}{(z_i e)^2 J_i^{\text{mass}} A}$$

$$I_i(n) = \Delta J_i^{\text{charge}}(\bar{x}_n,\omega)A; .....0 \le n \le N-1$$

$$I_{\text{dis}}(n) = \Delta J_{\text{dis}}^{\text{charge}}(\bar{x}_n,\omega)A; .....0 \le n \le N-1$$

$$V_i(n) = \Delta\tilde{\mu}_i^*(x_n,\omega); .....0 \le n \le N$$

$$V_{\text{dis}}(n) = \Delta\phi(x_n,\omega); .....0 \le n \le N$$

$$V_i(n) - V_{\text{dis}}(n) = \Delta\mu_i^*(x_n,\omega); .....0 \le n \le N$$

$$I_i^0(n) = \frac{V_i(n)-V_{\text{dis}}(n)}{Z_i^0}; .....0 \le n \le N \tag{109}$$

Interpretation of several of the terms in (109) is immediately possible by direct inspection. It is apparent, for example, that R_i in (109) is the (mean) resistance of carrier i in volume element n and C_{dis} is the dielectric capacitance of the element. The term I_i is simply the perturbation current flowing through resistor R_i and I_{dis} is the perturbation displacement current flowing through the capacitor C_{dis}. The term C_i^{chem} is the

"chemical capacitance" of carrier i. This quantity reflects the ability of the system to store chemical energy in the form of changes in stoichiometry in response to changes in chemical potential and has been discussed at length elsewhere.[13] The voltage terms, V_i, V_{dis} and $V_i - V_{\text{dis}}$ correspond simply to perturbations in the reduced electrochemical potential, the electrical potential and the reduced chemical potential, respectively. In addition to these elements, which are encountered relatively frequently in the solid state ionics literature, two new terms, Z_i^0 and I_i^0 appear in (109). The first, Z_i^0 (or R_i^0) is a frequency-independent "source resistance" caused by the constant flux, J_i^{mass}, which is nonvanishing in a mixed conductor exposed to a chemical potential gradient. The second, I_i^0, is a voltage-dependent current source, where the magnitude of the perturbation flux is directly proportional to the magnitude of the perturbation in chemical potential gradient driving the current. The distinction between this behavior and that of a passive resistor element is described more fully below.

Using Kirchoff's laws,[23] the reformulated transport eqns (105)–(109) can further be mapped to an equivalent circuit, the result of which is presented in Fig. 6a for a single element in the grid system and for the specific case of the two-carrier material considered here. This circuit bears a strong resemblance to that recently presented for MIECs under uniform chemical potential conditions,[13,14] Fig. 6b, in that two carrier rails run in parallel with a displacement rail, with the carrier rails each coupled to the displacement rail *via* chemical capacitors. However, in addition to passive resistor (R_i) and capacitor (C_{dis}, C_i^{chem}) elements, the equivalent circuit under potential gradient conditions contains the newly derived active elements, I_i^0, voltage-controlled current sources. As evident from eqn (105), there are three current terms that contribute to the ionic current through element n shown in Fig. 6a. The first is the conventional ohmic current resulting from the electrical potential difference between points C and E. The additional terms, $I_{\text{ion}}^0(n)$ and $I_{\text{ion}}^0(n+1)$, as defined in (109), are, respectively, proportional to the voltage differences between points C and D, and between points E and F rather than to the voltage difference across the element (*i.e.*, points C and E, as the ohmic current is). The "voltage" difference between points along the carrier rails and the displacement rail is, as also defined in (109), in fact, the perturbation in chemical potential experienced by the mobile species. Thus, while Ohm's law describes the flow of charge in response to an applied electrical potential gradient, it is apparent here that there is also a flow of charge in response to a perturbation in the chemical potential field.

The validity of this formulation can be evaluated by examining the behavior under equilibrium conditions $J_i^{\text{mass}} = 0$, which must reduce to the earlier literature results for mixed conductors under uniform atmospheres.[13,14] Under such conditions, because the mass flux is zero, the voltage controlled current source of (109) is also zero, explicitly

$$I_i^0(n) = 0 \tag{110}$$

Eqn (105) thus becomes

$$I_i(n) = -\frac{V_i(n+1) - V_i(n)}{Z_i(n+1)} \tag{111}$$

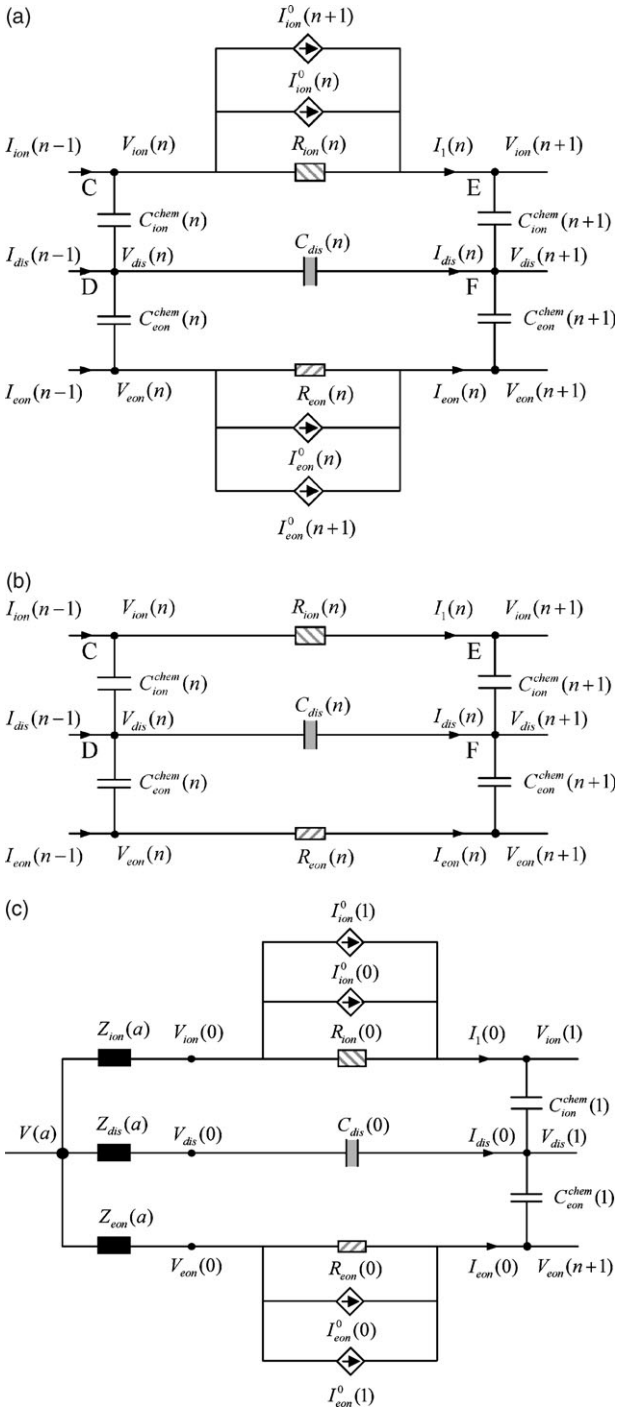

Fig. 6 AC equivalent circuits for the volume elements of a mixed conductor under selected conditions: (a) a bulk element under a chemical potential gradient ($1 \leq n \leq N-1$); (b) a bulk element under uniform chemical potential ($1 \leq n \leq N-1$); (c) a boundary element under a chemical potential gradient ($n = 0$).

and the equivalent circuit indeed reduces to the appropriate form.

It is to be emphasized that, in fact, equilibrium conditions can never be attained in a mixed conductor exposed to a chemical potential gradient because the flux in such a system will always be non-zero. That is, whereas fixed partial pressures in the anode and cathode chambers (achieved *via* a

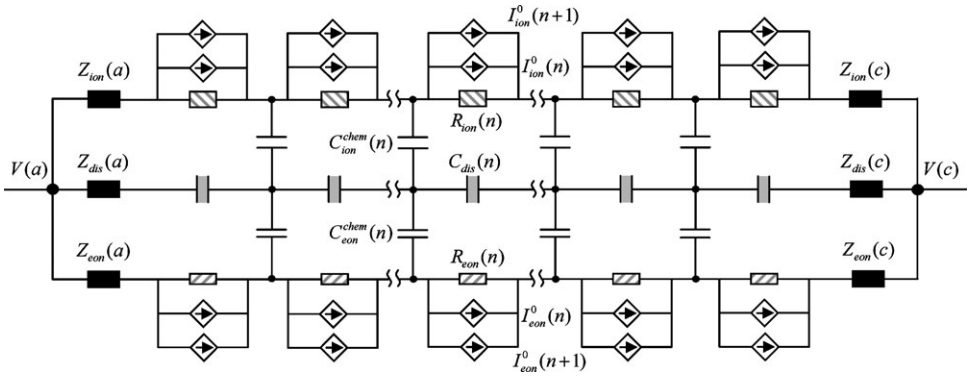

Fig. 7 Complete AC equivalent circuit for a mixed conductor including the electrodes, under a chemical potential gradient.

constant flow of gases) can generate steady state conditions, the system, by definition, cannot equilibrate. The non-zero flux, in turn, is responsible for the occurrence of the new equivalent circuit elements in the physical representation of the mixed conductor. For these reasons the equivalent circuit derived for a mixed conductor exposed to a uniform chemical potential (and thus equilibrium conditions) can not be directly applied to represent the electrochemical behavior of mixed conductors exposed to chemical potential gradients.

2.4.2 Numerical solution for arbitrary boundary conditions

As already shown, under steady state conditions it is possible, by making use of the constant vacancy approximation, to derive analytical expressions for quantities such as the electron concentration profile, the oxygen chemical potential, *etc.* Under a small signal perturbation, given the complexity of the equations given in (105)–(109) it is not obvious what approximations would be required in order to obtain analogous analytical solutions. Instead, a numerical methodology is pursued here to derive the solutions for the position dependent quantities. The approach has the benefit of being directly compatible with any arbitrary set of boundary conditions, and this aspect is discussed first.

At the boundary, the circuit, comprising N elements of the form depicted in Fig. 6a, is terminated at the anode (and analogously at the cathode) as shown in Fig. 6c, where $V_{\mathrm{ion}}(0)$, $V_{\mathrm{dis}}(0)$ and $V_{\mathrm{eon}}(0)$ are unknown voltage drops in the ionic, discharge and electronic rails, respectively. These rails are not coupled to one another *via* the chemical capacitors at the boundaries because the continuity equation is not applicable at these locations. The electrode characteristics are embodied in the phenomenological functions $Z_{\mathrm{ion}}(a)$, $Z_{\mathrm{dis}}(a)$ and $Z_{\mathrm{eon}}(a)$, which can represent any level of complexity in the electrochemical reaction pathways. Mathematically, they are the small signal perturbations to the boundary functions g and h introduced in section 2.2. Considering both electrodes, the boundary conditions can be written as

$$\begin{aligned} V(a) - V_i(0) &= Z_i(a)I_i(0) \\ V(a) - V_{\mathrm{dis}}(0) &= Z_{\mathrm{dis}}(a)I_{\mathrm{dis}}(0) \\ V_i(N) - V(c) &= Z_i(c)I_i(N) \\ V_{\mathrm{dis}}(N) - V(c) &= Z_{\mathrm{dis}}(c)I_{\mathrm{dis}}(N) \end{aligned} \tag{112}$$

where $Z_i(a)$, Z_i (c), $Z_{\mathrm{dis}}(a)$ and $Z_{\mathrm{dis}}(c)$ are the boundary impedances as already described, $V(a)$ and $V(c)$ are the (input) boundary voltages at the anode and cathode, respectively, and i, as already discussed, refers to the species. The complete equivalent circuit including the electrodes is shown in Fig. 7.

Expressions (105), (106), (107), (108), and (112) can, respectively, be rewritten by simply algebraic manipulation as

$$\begin{aligned} &[Z_i^0 + Z_i(n)]V_i(n) + [Z_i(n) - Z_i^0]V_i(n+1) \\ &- Z_i(n)V_{\mathrm{dis}}(n) - Z_i(n)V_{\mathrm{dis}}(n+1) \\ &- Z_i(n)Z_1^0 I_i(n) = 0; \ldots\ldots 0 \le n \le N-1 \end{aligned} \tag{113}$$

$$\begin{gathered} V_i(n) - V_{\mathrm{dis}}(n) - Z_i^{\mathrm{chem}}(n)I_i(n-1) + Z_i^{\mathrm{chem}}(n)I_i(n) = 0; \\ 1 \le n \le N-1 \end{gathered} \tag{114}$$

$$\begin{gathered} V_{\mathrm{dis}}(n) - V_{\mathrm{dis}}(n+1) - Z_{\mathrm{dis}}(n)I_{\mathrm{dis}}(n) = 0; \\ 1 \le n \le N-1 \end{gathered} \tag{115}$$

$$\begin{gathered} \sum_i [I_i(n-1) - I_i(n)] + I_{\mathrm{dis}}(n-1) - I_{\mathrm{dis}}(n) = 0; \\ 1 \le n \le N-1 \end{gathered} \tag{116}$$

$$\begin{aligned} -V_i(0) - Z_i(a)I_i(0) &= -V(a) \\ -V_{\mathrm{dis}}(0) - Z_{\mathrm{dis}}(a)I_{\mathrm{dis}}(0) &= -V(a) \\ V_i(N) - Z_i(c)I_i(N) &= V(c) \\ V_{\mathrm{dis}}(N) - Z_{\mathrm{dis}}(c)I_{\mathrm{dis}}(N) &= V(c) \end{aligned} \tag{117}$$

Because there are two mobile species under consideration for SDC, oxygen vacancies and electrons, these expressions imply a set of $6N + 3$ equations, in $6N + 3$ terms. Accordingly, they can be written in matrix form as

$$\boldsymbol{AX} = \boldsymbol{B} \tag{118}$$

where $\boldsymbol{A}$ is a $(6N + 3) \times (6N + 3)$ sparse matrix with elements of $Z_i(n)$, $Z_{\mathrm{dis}}(n)$, $Z_i^{\mathrm{chem}}(n)$, Z_i^0, $Z_i(a)$, $Z_i(c)$, $Z_{\mathrm{dis}}(a)$ and $Z_{\mathrm{dis}}(c)$; $\boldsymbol{B}$ is a $6N + 3$ column vector with only six non-zero elements, $\pm V(a)$ and $\pm V(c)$; and $\boldsymbol{X}$ is a $6N + 3$ column vector with elements of $I_i(n)$, $I_{\mathrm{dis}}(n)$, $V_i(n)$ and $V_{\mathrm{dis}}(n)$. The terms in $\boldsymbol{B}$ are

given by the experimental input voltage. The terms in $\boldsymbol{A}$ are, in principle, unknown because the material properties depend on the unknown concentration profiles, *etc*., however, their values can be estimated from the steady state solution and some assumed behavior of the electrodes. With $\boldsymbol{A}$ and $\boldsymbol{B}$ as known quantities, the solution to the small signal problem reduces to finding the solution for the matrix $\boldsymbol{X}$, a mathematically tractable problem.

Of particular interest in the small signal solution is the impedance, $Z(\omega)$. This quantity can be calculated from the ratio of the perturbation voltage to the perturbation current, according to

$$Z(\omega) = \frac{V(a) - V(c)}{\Delta J_{\mathrm{T}}^{\mathrm{charge}}(\omega) A} = \frac{V(a) - V(c)}{I_{\mathrm{ion}}(1) + I_{\mathrm{eon}}(1) + I_{\mathrm{dis}}(1)} \quad (119)$$

where, for ease, the flux terms are evaluated at the first element.

It is of value to note that mixed conductors exposed to a chemical potential gradient may be considered to be ''purely'' ionic under some range of the applied chemical potential. This situation certainly applies to doped ceria which, at moderate temperatures, is considered a ''pure'' ionic conductor at the cathode and a mixed conductor at the anode. The analysis here emphasizes that even under oxidizing conditions, the resistance to electronic transport cannot be infinite. The electron flux at the oxidized side of the electrolyte must be exactly equal to that at the reduced side. For this reason, the electronic carrier rail extends completely across the length of the sample from $x = 0$ to $x = L$.

3. Experimental procedure

3.1 Data acquisition

The bulk of the electrochemical data were collected from $Sm_{0.15}Ce_{0.85}O_{1.925-\delta}$ (SDC15) based cells configured with $Ba_{0.5}Sr_{0.5}Co_{0.8}Fe_{0.2}O_{3-\delta}$ (BSCF) as the cathode and Pt as the anode. Additional data were also obtained from symmetric cells of BSCF|SDC15|BSCF and Pt|SDC15|Pt.

Commercial $Sm_{0.15}Ce_{0.85}O_{1.925}$ (SDC15) powders were purchased from NexTech Materials Ltd. They were first calcined at 950 °C in air for 5 h in order to lower the surface area and obtain the desired sintering characteristics and then uniaxially pressed at 300 MPa to form pellets. These were sintered at 1350 °C for 5 h, to yield samples with relative densities of over 95%. The samples used for measurement were between 0.6 and 0.7 mm in thickness with a diameter of approximately 13 mm.

The BSCF cathode material was prepared in-house by a sol-gel method in which both EDTA and citric acid served as chelating agents. Complete details are provided elsewhere.[24] The resulting powder was mixed with α-terpineol (Alfa Aesar), 0.1 ml liquid to 100 mg powder, to form a paste, which was then brush-painted onto the SDC pellet and fired at 1075 °C for 5 h. The Pt electrodes consisted of a commercial ink (Engelhard 6082), which was also applied by brush painting and then fired at 900 °C for 2 h. In the case of the symmetric cells, the electrodes were applied so as to completely cover the faces of the SDC pellets. In the case of the asymmetric cell, the electrode area was limited to a diameter of 10 mm. The cell was then sealed onto an alumina tube with an inner diameter of around 9.5 mm and a outer diameter of 12.5 mm, using an alumina-based adhesive (Aremco, Cerambond 552-VFG). All experiments on both symmetric and asymmetric cells were carried out in a two point configuration, using silver mesh current collectors with silver paste and silver wire leads.

Electrical characterization by AC impedance spectroscopy of all three cells was performed under uniform, oxidizing conditions, in addition to chemical potential gradient conditions for the asymmetric cell. Measurements were performed at selected temperatures between 550 and 650 °C, depending on the particular experiment. The oxidizing conditions were achieved by flowing synthetic air (Ar + O_2) at a rate of 100 ml/min to unsealed symmetric cells or to both sides of the sealed asymmetric cell. The chemical potential gradient experiments were performed by supplying either oxygen or synthetic air to the cathode (O_2 or Ar + O_2, at a total flow rate of 100 ml/min) and Ar + H_2 mixtures (with Ar:H_2 ratios of 0:100; 50:50; 80:20; and 90:10, and total flow rate of 50 ml/min), saturated with 3% H_2O at the anode. The oxygen partial pressure in the anode chamber was calculated assuming thermodynamic equilibrium between O_2, H_2 and H_2O. Gas flow rates for all experiments were controlled by MKS mass flow controllers.

The electrochemical data were collected using a Solartron 1260A frequency response analyzer in combination with a Princeton Applied Research EG&G 273A potentiostat/galvanostat. Both the voltage under open circuit conditions and the electrical impedance response were measured. In the latter case, the applied voltage amplitude was 10 mV (potentiostatic mode) and the frequency measurement range was 1 mHz–65 kHz. At each condition, the sample was allowed to equilibrate for at least 30 minutes before recording the data. At the lower temperatures the electrode resistance became exceedingly large under mildly oxidizing conditions, limiting the acquisition of meaningful data to highly reducing conditions. It was observed that, for the combination of sample processing conditions employed and electrical characterization temperatures probed, grain boundary effects were absent from the impedance spectra.[14]

3.2 Data analysis

Analysis of the impedance spectra measured under chemical potential gradient conditions in terms of the procedure outlined in section 2.4.2 required the values for several physical quantities as input parameters, and they were obtained as follows. The lattice constant of SDC15 was determined from Rietveld structure refinement utilizing powder X-ray diffraction data collected using a Philips X'Pert Pro diffractometer (Cu Kα radiation) over the 2θ range 20–100°. Nickel was employed as an internal 2θ standard. The coefficient of thermal expansion and the relative dielectric constant were taken to be 12.1 ppm and 11, respectively, after ref. 25. The electronic conductivity and equilibrium reduction constant were taken from ref. 26. The active area of the asymmetric cell was also considered an unknown because of the difference between the electrode and electrolyte areas. This area was determined from a comparison of the ionic conductivities

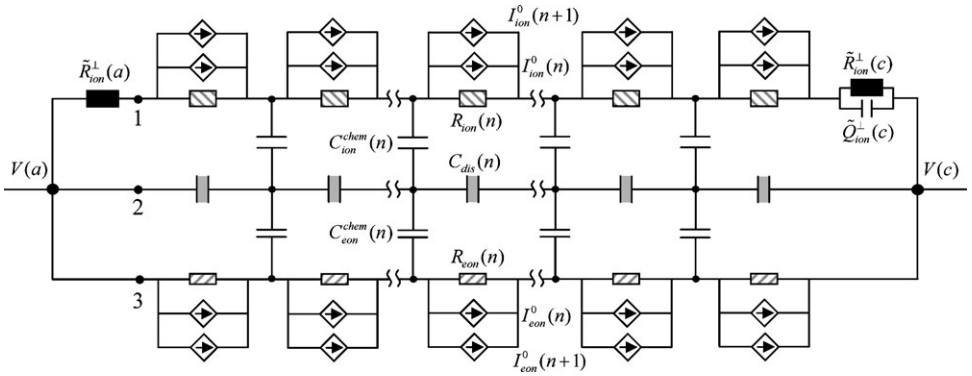

Fig. 8 Simplified AC equivalent circuit used to fit to the experimental data of Pt|SDC|BSCF. See text for discussion of marked points (1), (2), and (3).

obtained at 650 °C from the symmetric Pt|SDC|Pt cell with well-defined geometry and from the asymmetric cell (as measured in both cases under oxidizing conditions).

The AC impedance data displayed measurable inductance effects which resulted from the electrode and wiring geometry, as well as a non-negligible ohmic resistance due to the lead wires. Given the level of accuracy required of the experimental data in order to extract the physical terms described here, particular care was aimed at minimizing the influence of these extraneous effects. Specifically, the lead wire resistances for the symmetric and asymmetric experimental configurations, R_0^{s} and R_0^{as}, were obtained from resistance measurements in which the apparatus was shorted at the sample location. These resistance values were subsequently treated as constants. To account for the inductance behavior, a freely fitted inductance term was included in all equivalent circuit models in addition to the fixed lead wire resistance term.

The AC impedance data collected under fuel cell conditions were analyzed in terms of the formalism outlined in section 2.4.2. First, the impedance boundary conditions were simplified from the general functions indicated in Fig. 7 to ones with limited numbers of free fitting parameters. The interfacial impedances of the electronic and discharge rails were taken to be zero, as justified by the high electronic conductivity of the Pt and BSCF electrodes; the interfacial impedance of the ionic rail was taken to behave as a resistor, $\tilde{R}^{\perp}_{ion}$, and constant phase element, $\tilde{Q}^{\perp}_{ion}$, in parallel with one another, where the impedance of a constant phase element is $Q = [(j\omega)^{\alpha}Y]^{-1}$ and the effective capacitance is $[Y]^{1/\alpha}[R]^{1/\alpha-1}$. The ''tilde'' here is used to emphasize that the quantities correspond to the small signal perturbations of the values under steady state conditions, rather than the steady state values themselves. Interfacial capacitance effects are captured *via* $\tilde{Q}^{\perp}_{ion}$ (explicitly in terms of the quantities $\tilde{Y}^{\perp}_{ion}$ and $\tilde{\alpha}^{\perp}_{ion}$). At the anode side, because the large electrolyte chemical capacitance overwhelms any influence of the interfacial capacitance, the latter was omitted from the analysis. The equivalent circuit under these assumptions reduces to that shown in Fig. 8. Although, in the most general case, electrodes cannot be described by this simple empirical representation, this model, as shown below, yields an impedance that fits the experimental data very well.

Some subtleties inherent in the equivalent circuit presented in Fig. 8 require comment. The driving force for charge transport along the charge carrier rails is the gradient in electrochemical potential, whereas that along the displacement rail is the gradient in electric potential field. Moreover, because the electric potential, $\Delta\phi$, is physically required to be single-valued at any location in the material, it has the same value at points 1, 2 and 3 indicated on the three different rails. Considering the anode, the absence of a terminal impedance along the electronic carrier rail implies that the electrochemical potential of electrons, $\Delta\tilde{\mu}^{*}_{eon}$, at the point labeled 3 is equal to that at the termination of the circuit at $V(a)$. Because a measurement of the voltage drop corresponds to changes in electron electrochemical potential, the absence of a terminal impedance further implies the absence of a voltage drop across the electrode|electrolyte interface, as previously discussed. The absence of a terminal impedance for the displacement rail, in turn, implies that there is no change in the electric field across the interface, *i.e.*, between point 2 and the termination of the circuit at $V(a)$. On the other hand, the occurrence of a terminal impedance along the ionic carrier rail implies that there is difference in the electrochemical potential of the ions between point 1 and the termination of the circuit at $V(a)$. In light of the absence of a change in electric field (no terminal impedance along the displacement rail) this electrochemical potential difference is simply equal to the chemical potential difference across the interface. Thus, the (RQ) terminal impedance along the ionic rail reflects the ''effective'' resistor and capacitance behavior in response to a chemical rather than electrical driving force. It is to be emphasized that the existence in the circuit of this terminal impedance does not contradict the statement that there is no voltage drop across the interface, a point already alluded to in the discussion of the steady state solution, section 2.3.2.

In accordance with these simplification to the equivalent circuit, six terms, $p_{O_2}(0)$, $p_{O_2}(L)$, $\tilde{R}^{\perp}_{ion}(c)$, $\tilde{Y}^{\perp}_{ion}(c)$, $\tilde{\alpha}^{\perp}_{ion}(c)$ and $\tilde{R}^{\perp}_{ion}(a)$, are to be specified to describe the electrochemical state of the system. Given the measured value of OCV, the first two terms are related according to eqn (76), leaving five independent terms to be determined from an analysis of the impedance data. To obtain these, arbitrary initial guesses were made for $p_{O_2}(L)$, $\tilde{R}^{\perp}_{ion}(c)$, $\tilde{Y}^{\perp}_{ion}(c)$, $\tilde{\alpha}^{\perp}_{ion}(c)$ and $\tilde{R}^{\perp}_{ion}(a)$, and the first of these terms, $p_{O_2}(L)$ was used, together with $p_{O_2}(0)$, to calculate an initial electron concentration profile within the electrolyte. With this, all the elements in matrix $\boldsymbol{A}$ of eqn (118)

are established. Upon solution of the matrix equation, which was accomplished here using the sparse matrix direct solver UMFPACK 4.6,[27–30] the impedance was evaluated according to eqn (119) for each measurement frequency, ω_m The calculated value, $Z_{calc}(\omega_m)$, was compared to that measured experimentally, $Z_{calc}(\omega_m)$, and the difference between the two iteratively minimized by the complex nonlinear least squares method using the Levenberg-Marquardt algorithm. Explicitly, the following function was minimized[31]

$$S = \sum_m \left[\left(\frac{\mathrm{Re}\, Z_{meas}(\omega_m) - \mathrm{Re}\, Z_{calc}(\omega_m)}{|Z_{calc}(\omega_m)|} \right)^2 + \left(\frac{\mathrm{Im}\, Z_{meas}(\omega_m) - \mathrm{Im}\, Z_{calc}(\omega_m)}{|Z_{calc}(\omega_m)|} \right)^2 \right] \quad (120)$$

where Re and Im represent, respectively, the real and imaginary parts of the impedance, the summation is over all experimental frequencies, and the square of the inverse modulus of the calculated impedance serves as the weighting function. The number of elements in the discretization, N, was set at 20 000, for which convergence was attained.

4. Results and discussions

The results of the open circuit voltage measurements are presented in Fig. 9 as a function of temperature for the conditions in which "100%" H_2 (saturated with 3% H_2O) was supplied to the anode. These values are compared in the figure to the Nernst and theoretical values, where, as already described, the Nernst values corresponds to what would be measured with a pure ionic conductor and the theoretical values correspond to what would be measured across SDC15 using ideal electrodes. The complete set of results is presented in Table 1. Returning to Fig. 9, the substantial decrease in all three voltage terms with increasing temperature is largely a result of the equilibrium between H_2, H_2O and O_2 generating less oxidizing conditions at the anode at high temperatures. As evident from the behavior of V_{oc}^{th}, the mixed conducting nature of SDC15 inherently causes a loss of open circuit voltage of 0.09 to 0.15 V under these conditions, whereas the non-ideality of the electrodes leads to even greater voltage losses, as evident from the behavior of the measured OCV. Similar results were obtained for the experiments with "50%", "20%" and "10%" H_2 at the anode, Table 1.

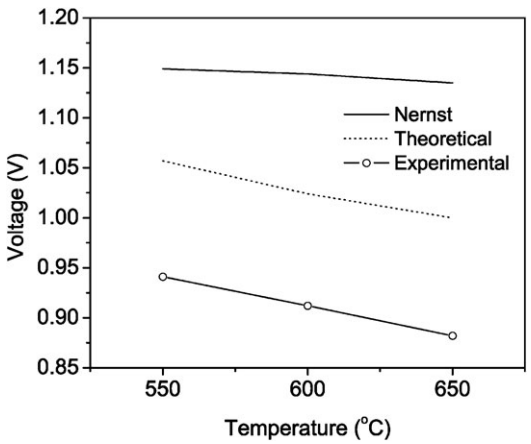

Fig. 9 Nernst, theoretical and experimental voltage values as functions of temperature. The cathode gas is synthetic air and the anode gas is "100%" H_2, supplied saturated with 3% H_2O.

Before presenting the impedance spectra of the asymmetric cell under fuel cell conditions, it is of value to consider the spectra of the symmetric, Pt-electroded cell under reducing conditions and of the symmetric, BSCF-electroded cell under oxidizing conditions. The behavior of the former has been discussed extensively in our previous work,[14] and, in brief, the spectra display a single, asymmetric, half-tear-drop shaped arc that is displaced from the origin, in complete agreement with the predictions of the Jamnik–Maier model.[12,14] The displacement along the real axis in the Nyquist representation corresponds primarily to the total bulk conductivity of the mixed conductor, whereas the half-tear-drop shaped (also termed Warburg-like) asymmetric arc broadly corresponds to the interfacial characteristics. Turning to the cathode material, the behavior of the BSCF-electroded symmetric cell is presented in Fig. 10 in the Nyquist representation (Re Z *vs.* $-$Im Z) for a measurement under synthetic air at 600 °C. In general agreement with previous studies,[24] the interfacial resistance between SDC and BSCF is small, amounting to 0.38 Ω cm^2 in this particular measurement. The observed arc displays slight asymmetry, but, in contrast to the Pt|SDC|Pt system, the data can be adequately described by a (RQ) subcircuit.

A typical impedance spectrum for the asymmetric Pt|SDC15|BSCF cell under fuel cell conditions (synthetic air supplied to the cathode and H_2 + 3% H_2O supplied to the anode) at 600 °C is presented in Fig. 11. In the Nyquist representation, Fig. 11(a), the spectrum appears to be composed of a large Warburg-like arc at low frequencies, a small apparently symmetric arc at higher frequencies, and an inductor at the highest frequencies. These characteristics can be readily understood to reflect the properties of the Pt|SDC interface under reducing conditions and the BSCF|SDC interface under oxidizing conditions. The solid lines in Fig. 11 are the values of the fit performed according to the procedures outline above, with a final value of the refinement statistic, S,

Table 1 Nernst, theoretical and experimental voltages for different temperatures and oxygen partial pressures

T °C	Anode H_2, %	$p_{O_2}(c)$ Atm	$p_{O_2}(a)$ atm	V_N V	V_{oc}^{th} V	V_{oc} V
650	100	0.21	3.42E-26	1.135	0.987	0.882
650	50	0.21	1.34E-25	1.108	0.982	0.867
650	20	0.21	8.72E-25	1.071	0.973	0.845
650	10	0.21	2.63E-24	1.049	0.966	0.830
600	100	0.21	8.30E-28	1.144	1.024	0.912
600	50	0.21	3.28E-27	1.118	1.018	0.897
600	20	0.21	2.13E-26	1.083	1.007	0.876
600	10	0.21	6.50E-26	1.062	0.998	0.862
600	100	1	8.30E-28	1.173	1.053	0.938
600	50	1	3.28E-27	1.147	1.047	0.922
600	20	1	2.13E-26	1.112	1.036	0.893
600	10	1	6.50E-26	1.091	1.028	0.875
550	100	0.21	1.50E-29	1.149	1.057	0.941
550	50	0.21	5.90E-29	1.125	1.050	0.926
550	20	0.21	3.84E-28	1.092	1.036	0.905
550	10	0.21	1.17E-27	1.072	1.027	0.890

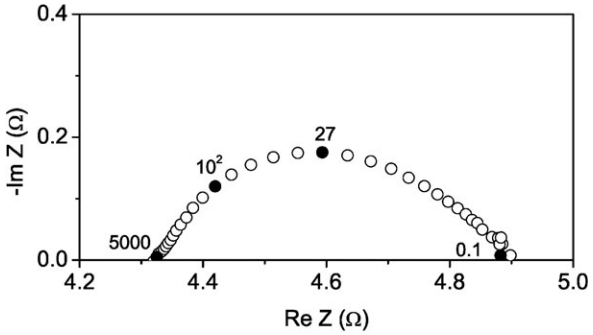

Fig. 10 Measured impedance response of BSCF|SDC15|BSCF under synthetic air at 600 °C. Numbers on the spectrum correspond to the frequency at the indicated point.

being 0.20%. Overall, it is evident that the model captures quite well the experimental behavior.

For each experimental condition, analysis of the OCV and impedance data were used, as already described, to determine the six terms $p_{O_2}(0)$, $p_{O_2}(L)$, $\tilde{R}^{\perp}_{ion}(c)$, $\tilde{Y}^{\perp}_{ion}(c)$, $\tilde{\alpha}^{\perp}_{ion}(c)$ and $\tilde{R}^{\perp}_{ion}(a)$. From (59), which relates the charge flux to the oxygen partial pressures at the electrode|electrolyte interfaces, the term J^{charge}_{ion} was evaluated, and using (80), which relates the oxygen partial pressure change across each interface to the effective interfacial resistance, the values of $\tilde{R}^{\perp}_{ion}(a)$ and $\tilde{R}^{\perp}_{ion}(c)$ were individually determined. For comparative purposes, the theoretical value of J^{charge}_{ion} was also calculated, in this case by using the values of the oxygen partial pressures in the anode and cathode chambers for the evaluation of (59). The complete set of results is presented in Table 2, along with the value of S for each fit. An example of the virtual oxygen potential profile, evaluated according to eqn (55), is presented in Fig. 12, where the calculation corresponds to the conditions of Fig. 11 (T = 600 °C, $p_{O_2}(0)$ = 0.21 atm, $p_{O_2}(a) = 8.30 \times 10^{-28}$ atm). Given that the derivation of eqn (55) is based on the steady state solutions already known in the literature, the behavior within the mixed conductor is typical. Across the thin electrodes, particularly the anode, the change in oxygen partial pressure is extremely steep, and appears on the scale of the figure as discontinuous.

Several aspects of the results summarized in Tables 1 and 2 are noteworthy. Consistent again with the high electrochemical activity of the BSCF cathode, the oxygen partial pressure drop from the cathode gas chamber, $p_{O_2}(c)$, to the cathode|electrolyte interface, $p_{O_2}(L)$, is rather small in relative terms, approximately 0.1 atm when synthetic air was supplied to the cathode and approximately 0.5 atm when oxygen was supplied. In contrast, at the Pt anode, there is a large oxygen partial pressure drop (around 5 orders of magnitude) from the anode gas chamber, $p_{O_2}(a)$, to the anode|electrolyte interface, $p_{O_2}(0)$. These oxygen partial pressure drops correspond to a loss in the OCV of about 0.01 and 0.22 V for the cathode and anode, respectively. The OCV loss due to the mixed conducting electrolyte is only on the order of 0.02 V, much lower than suggested by Fig. 9 because the oxygen partial pressure at the electrolyte|anode interface is much larger than in the anode chamber.

The precise values of the oxygen partial pressures at the electrode|electrolyte interfaces depend strongly on the oxygen partial pressures within the electrode chambers. Overall, as the oxygen partial pressure of the anode chamber, $p_{O_2}(a)$, was raised, that at the anode|electrolyte interface, $p_{O_2}(0)$, increased, and, similarly, with increasing $p_{O_2}(c)$, $p_{O_2}(L)$ increased, much as would be expected. Examining the correlations across the electrolyte, it is evident that as the oxygen partial pressure in the cathode chamber was increased from 0.21 to 1 atm (at 600 °C), the value at the anode|electrolyte interface, $p_{O_2}(0)$, also increased slightly, an intuitively satisfying response. In contrast, as the oxygen partial pressure in the anode chamber, $p_{O_2}(a)$, was increased (at a given temperature), the oxygen partial pressure at the cathode|electrolyte interface, $p_{O_2}(L)$, *decreased*, with just one exception, when the cathode gas was synthetic air, the anode gas H_2 + 3% H_2O, and the temperature 650 °C. Because the contribution of the cathode impedance to the overall system impedance is small, the possibility that this effect is an artifact of the fitting procedures cannot be entirely ruled out. However, such artifacts are considered unlikely given the excellent agreement between the model and the measured impedance data. Furthermore, the physically related, but numerically independent parameter, $\tilde{R}^{\perp}_{ion}(c)$ (increasing with increasing $p_{O_2}(a)$) displays an analogous trend. Physically, such behavior can plausibly be the result of a sharp increase in the cathode interfacial resistance in response to an increase in the oxygen chemical potential. That is, if the material properties

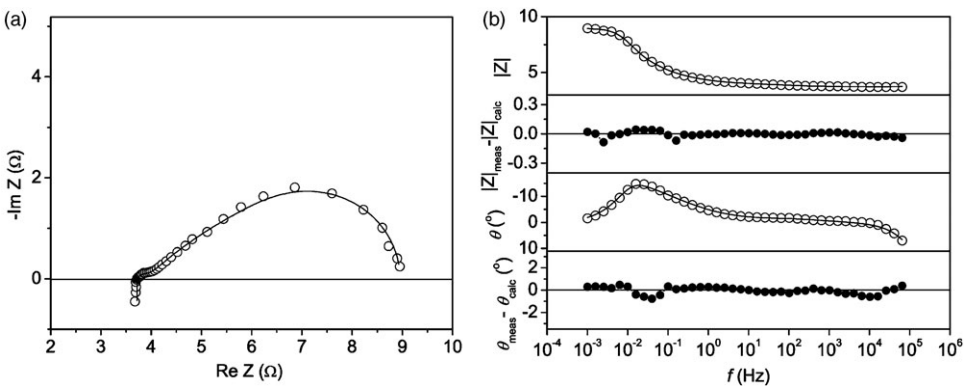

Fig. 11 Comparison of the measured and fit impedance obtained from the Pt|SDC15|BSCF system at conditions T = 600 °C, $p_{O_2}(c)$ = 0.21 atm (synthetic air) and $p_{O_2}(a) = 8.3 \times 10^{-28}$ atm ("100% H_2" with 3% H_2O). (a) Nyquist representation, and (b) Bode–Bode representation.

Table 2 Results for the interfacial oxygen partial pressures, electrode resistances, charge fluxes from fitting to the experimental impedance spectra and the experimental open circuit voltage. The interfacial oxygen partial pressures, $p_{O_2}(L)$ and $p_{O_2}(0)$, and the perturbation values of the interfacial resistances at the electrolytes, $\tilde{R}^{\perp}_{ion}(c)$ and $\tilde{R}^{\perp}_{ion}(a)$, were obtained directly from the experimental data. The effective interfacial resistances, $R^{\perp}_{ion}(c)$ and $R^{\perp}_{ion}(a)$, were determined from the interfacial oxygen partial pressures using (80). The flux J^{charge}_{ion} is the experimentally implied flux based on the measured OCV, whereas $J^{charge,\ th}_{ion}$ is the theoretical flux under the conditions of ideally active electrodes. S is the goodness of fit to the impedance spectra

T °C	Anode H_2, %	$p_{O_2}(c)$ atm	$p_{O_2}(L)$ Atm	$p_{O_2}(0)$ atm	$R^{\perp}_{ion}(c)$ Ω	$R^{\perp}_{ion}(a)$ Ω	$\tilde{R}^{\perp}_{ion}(c)$ Ω	$\tilde{R}^{\perp}_{ion}(a)$ Ω	J^{charge}_{ion} A/m^2	$J^{charge,\ th}_{ion}$ A/m^2	S %
650	100	0.21	0.121	2.00E-21	1.154	23.147	0.092	5.177	103.63	642.08	0.57
650	50	0.21	0.139	6.36E-21	1.127	29.268	0.094	7.067	80.38	545.42	0.31
650	20	0.21	0.128	2.23E-20	1.795	36.648	0.115	11.027	60.52	424.19	0.33
650	10	0.21	0.122	5.09E-20	2.391	43.153	0.120	14.618	50.00	359.83	0.51
600	100	0.21	0.126	4.45E-23	2.181	46.785	0.194	11.501	48.11	334.91	0.20
600	50	0.21	0.120	1.11E-22	2.956	55.136	0.224	15.628	39.12	279.53	0.22
600	20	0.21	0.114	3.88E-22	4.329	69.142	0.238	23.386	29.33	211.93	0.48
600	10	0.21	0.101	7.92E-22	6.082	78.428	0.255	31.087	24.80	176.60	0.54
600	100	1	0.563	5.12E-23	2.548	48.883	0.169	11.927	46.64	334.91	0.29
600	50	1	0.550	1.40E-22	3.329	59.435	0.185	16.015	37.09	279.53	0.33
600	20	1	0.434	6.37E-22	6.615	81.611	0.226	24.126	26.10	211.93	0.60
600	10	1	0.378	1.59E-21	9.562	99.428	0.221	31.288	21.01	176.60	0.79
550	100	0.21	0.129	5.80E-25	4.642	100.756	0.475	28.527	20.43	152.71	0.38
550	50	0.21	0.116	1.37E-24	6.952	117.021	0.536	39.311	16.74	124.84	0.36
550	20	0.21	0.092	4.08E-24	12.340	139.374	0.572	61.760	12.96	91.86	0.56
550	10	0.21	0.070	7.69E-24	19.120	153.649	0.596	81.714	11.15	75.21	1.02

governing the electrochemical reaction rate are inherently dependent on the oxygen chemical potential, the requirement that the flux be constant across the system can lead to this type of unusual solution of the transport equations. While a physical explanation can be hypothesized, a detailed study of the behavior of the BSCF cathode was not the objective of this study and this point is not discussed further.

In order to understand the significance of the variations in the resistance terms with experimental conditions, it is of value to understand the relationship between $\tilde{R}^{\perp}_{ion}$ and $R^{\perp}_{ion}$. As stated previously, the former is the perturbation value of the latter. Schematically, the measurement can be described as shown in Fig. 13. Here, a difference in electrochemical potential, $\Delta\tilde{\mu}^{*}_{ion}(a,0) = \tilde{\mu}^{*}_{ion}(a) - \tilde{\mu}^{*}_{ion}(0)$, across an interface (as indicated here for the anode) drives an electrochemical reaction to generate a flux. The "Δ" here does not refer to the perturbation in electrochemical potential. The functional dependence of the flux on the driving potential is arbitrary, but as discussed in section 2.2 several expressions have been considered in the literature, with the Butler-Volmer equation being most commonly assumed in electrochemical studies. The term $\tilde{R}^{\perp}_{ion}$ corresponds to the ratio between the total flux and the total electrochemical potential drop across the interface at the experimental conditions (*i.e.*, at the point *P*), whereas the term $\tilde{R}^{\perp}_{ion}$ corresponds to the inverse of the slope of the function, again at the specified point, *P*. Under uniform chemical potential conditions, the perturbations are applied about zero flux, and hence such measurements (not performed as part of this study) yield the inverse of the slope of the function about the origin, which we define here as $\tilde{R}^{\perp}_{ion}|_{J=0}$. Thus, it is apparent that the specific manner in which these three terms are related to one another depends on the details of the functional form of $J[\Delta\tilde{\mu}^{*}_{ion}(a,0)]$. Nevertheless, one can generally expect that they will be positively correlated, such that conditions which increase one will also increase the other two.

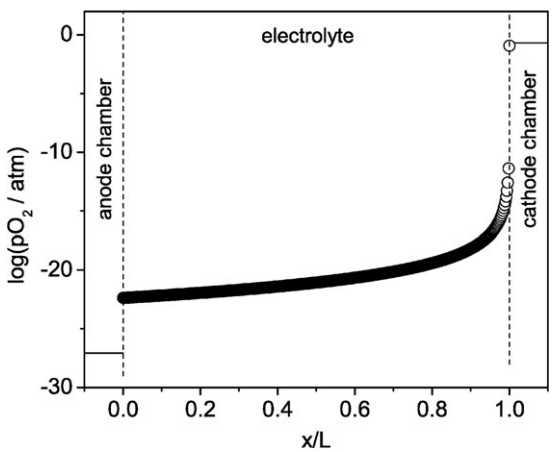

Fig. 12 Oxygen potential profile across Pt|SDC15|BSCF at conditions $T = 600$ °C, $p_{O_2}(c) = 0.21$ atm (synthetic air) and $p_{O_2}(a) = 8.3 \times 10^{-28}$ atm ("100% H_2" with 3% H_2O).

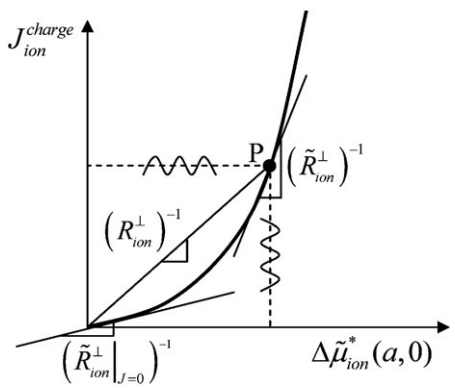

Fig. 13 Schematic relationship between current and electrochemical overpotential. The slope at point *P* corresponds to $(\tilde{R}^{\perp}_{ion})^{-1}$, the slope of line extending the origin to *P* corresponds to $(R^{\perp}_{ion})^{-1}$ and the slope at the origin corresponds to $(\tilde{R}^{\perp}_{ion|j=0})^{-1}$.

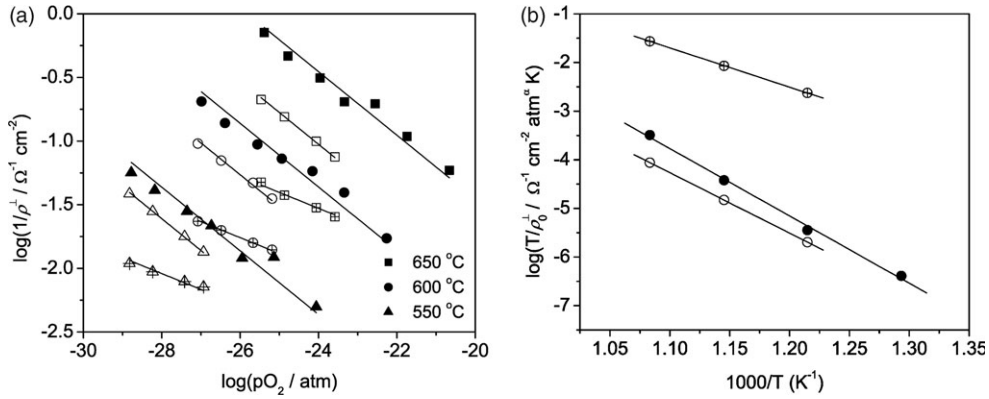

Fig. 14 (a) Inverse of the area specific electrode resistances of Pt in Pt|SDC15|BSCF, $\tilde{\rho}^{\perp}$ (open symbols) and $\rho^{\perp}$ (open-crossed symbols) under different anode atmospheres. For comparison, the inverse of the area specific electrode resistance obtained from Pt in Pt|SDC15|Pt from symmetric cell measurements (ref. 14 uniform atmosphere), $\tilde{\rho}^{\perp}|_{J=0}$, is also plotted (closed symbols). (b) Inverse of the oxygen partial pressure independent term in area specific electrode resistances of Pt in Pt|SDC15|BSCF as a function of temperature. Data are plotted in an Arrhenius form. Again, open, open-crossed and closed symbols are for $\tilde{\rho}^{\perp}$, $\rho^{\perp}$ and $\tilde{\rho}^{\perp}|_{J=0}$, respectively, taking the respective n values in the $p_{O_2}{}^n$ dependences to be $-1/4$, $-1/8$, and $-1/4$.

From an examination of the data in Table 2, it is apparent that there is indeed a correlation both between $\tilde{R}^{\perp}_{ion}(c)$ and $R^{\perp}_{ion}(c)$ and between $\tilde{R}^{\perp}_{ion}(a)$ and $R^{\perp}_{ion}(a)$, with two slight exceptions in the case of the cathode. Furthermore, it is apparent that $\tilde{R}^{\perp}_{ion}$ is substantially smaller than $R^{\perp}_{ion}$ for all conditions, by a factor of about three or four for the anode and as much as a factor of forty for the cathode. While a complete determination of the functional form of $J[\Delta\tilde{\mu}^{*}_{ion}(a,0)]$ or $J[\Delta\tilde{\mu}^{*}_{ion}(c,L)]$ is beyond the scope of the present work, the observed behavior is generally consistent with the Butler-Volmer type kinetics, with the slope of the *I–V* curve increasing with increasing overpotential. However, any rate-limiting step with non-linear behavior can also give rise to this behavior.

For the anode, because several different anode atmospheres were utilitized, it is possible to examine the dependence of $\tilde{R}^{\perp}_{ion}(a)$ and $R^{\perp}_{ion}(a)$ on oxygen partial pressure. This behavior can further be directly compared to the results we have obtained previously from Pt|SDC15|Pt cells under uniform chemical potentials at reducing conditions. Such a comparison is presented in Fig. 14(a) (limited to those experiments in which the cathode was supplied with synthetic air), where the $R^{\perp}_{ion}(a)$ values are converted to area specific terms, $\rho^{\perp} = AR^{\perp}_{ion}(a)$, and the inverse of $\rho^{\perp}$ is plotted *versus* p_{O_2} in log–log form. The quantities $\rho^{\perp}$, $\tilde{\rho}^{\perp}$, and $\tilde{\rho}^{\perp}|_{J=0}$ correspond, respectively, to $R^{\perp}_{ion}(a)$, $\tilde{R}^{\perp}_{ion}(a)$ and $\tilde{R}^{\perp}|_{J=0}$, with the latter as previously measured.[14] It is immediately evident that $\tilde{\rho}^{\perp}$ and $\tilde{\rho}^{\perp}|_{J=0}$ depend on oxygen partial pressure in the same manner, with the inverse of each being proportional to $p_{O_2}{}^{-1/4}$. In contrast, the term $\rho^{\perp}$, although also decreasing with decreasing oxygen partial pressure with a $p_{O_2}{}^n$ form ($n < 0$), displays a weaker dependence on oxygen partial pressure. The exponent in the fit ranges between -0.15 and -0.10, which we take to reflect a perhaps physically significant slope of $-1/8$. From a fit to the general form $1/\rho^{\perp} = (1/\rho^{\perp}_0)p_{O_2}{}^n$, where n is either $-1/4$ or $-1/8$, we obtain the corresponding oxygen partial pressure independent terms. Each of the $1/\rho^{\perp}_0$ terms has an Arrhenius temperature dependence, Fig. 14b, with activation energies of 1.60, 2.46 and 2.75 eV, respectively, for $R^{\perp}_{ion}(a)$, $\tilde{R}^{\perp}_{ion}(a)$ and $\tilde{R}^{\perp}_{ion}|_{J=0}$. In our earlier study, because of the similarity of the temperature and oxygen partial pressure dependences of $(\tilde{R}^{\perp}_{ion}|_{J=0})^{-1}$ with those of the electronic conductivity of SDC ($\sigma_{eon} = \sigma^{0}_{eon}p_{O_2}{}^{-1/4}$, $E = 2.44$ eV), we proposed that the electrochemical oxidation of hydrogen occurs directly on the surface of ceria, with the removal of electrons from the ceria surface to the Pt current collector being the rate limiting step. The observation that $\tilde{R}^{\perp}_{ion}(a)$ behaves in a manner almost identical to $\tilde{R}^{\perp}_{ion}|_{J=0}$ lends some support to the notion that this mechanism for hydrogen electro–oxidation also holds true under fuel cell conditions. The much greater value of $\tilde{R}^{\perp}_{ion}(a)$ over $\tilde{R}^{\perp}_{ion}|_{J=0}$ is likely a result of microstructural differences between samples rather than extreme non-linearities in the electronic conductivity of ceria. The distinctive behavior of $R^{\perp}_{ion}(a)$ relative to the other two interfacial resistance terms may, however, reflect a more complex reaction pathway.

Final points of consideration are the "internal short circuit" current densities, J^{charge}_{ion} and $J^{charge,th}_{ion}$, reported in Table 2. The former corresponds directly to the flux of oxygen ions across the mixed conducting electrolyte which cannot contribute to the electrical energy output of a fuel cell composed of the three component materials utilized here. The summary in Table 2 emphasizes the need to restrict operation of SDC based fuel cells to temperatures of 550 °C or less in order to limit losses due to electronic conductivity. More relevant to the present study, the data also reveal that ideally active electrodes would, in fact, increase the internal short-circuit density by increasing the oxygen partial pressure gradient across the membrane. The difference between the actual value of the flux for the electrodes utilized here and the ideal-electrode case is as much as a factor of seven.

5. Conclusions

A method for obtaining the small signal impedance solution for a mixed conductor exposed to a chemical potential

gradient that induces a gradient in carrier concentration is presented. Overall, the experimental data, obtained from the system Pt|SDC|BSCF, are well described by this first principles model. The analysis yields both the perturbation values of the electrochemical interfacial impedances and the oxygen partial pressure drops between the electrode chambers and the respective electrode|electrolyte interfaces. While a detailed study of interfacial properties is not the goal of this work, the observation that the perturbation term in the electrochemical impedance of the Pt|SDC15 interface displays similar temperature and oxygen partial pressure dependences as that measured previously for Pt|SDC|Pt under uniform, reducing conditions, suggests that the electrochemical reaction mechanisms may be similar for the two conditions, specifically, that electron migration through SDC15 is the rate-limiting step in hydrogen electro-oxidation.

Acknowledgements

The authors are grateful to Francesco Ciucci in Mechanical Engineering at the California Institute of Technology for discussions on the steady state solutions.

References

1 N. S. Choudhury and J. W. Patterson, *J. Electrochem. Soc*., 1971, **118**, 1398–1403.
2 C. Wagner, *Prog. Solid State Chem*., 1975, **10**, 3–16.
3 D. S. Tannhauser, *J. Electrochem. Soc*., 1978, **125**, 1277–1282.
4 I. Riess, *J. Electrochem. Soc*., 1981, **128**, 2077–2081.
5 S. Yuan and U. Pal, *J. Electrochem. Soc*., 1996, **143**, 3214–3222.
6 M. L. Liu, *J. Electrochem. Soc*., 1997, **144**, 1813–1834.
7 H. Nafe, *J. Electrochem. Soc*., 1997, **144**, 3922–3929.
8 R. Singh and K. T. Jacob, *J. Appl. Electrochem*., 2003, **33**, 571–576.
9 Z. Chen, *J. Electrochem. Soc*., 2004, **151**, A1576–A1583.
10 I. Riess, M. Godickemeier and L. J. Gauckler, *Solid State Ionics*, 1996, **90**, 91–104.
11 A. V. Virkar, *J. Power Sources*, 2005, **147**, 8–31.
12 J. Jamnik and J. Maier, *J. Electrochem. Soc*., 1999, **146**, 4183–4188.
13 J. Jamnik and J. Maier, *Phys. Chem. Chem. Phys*., 2001, **3**, 1668–1678.
14 W. Lai and S. M. Haile, *J. Am. Ceram. Soc*., 2005, **88**, 2979–2997.
15 I. D. Raistrick, D. R. Franceschetti and J. R. Macdonald, in *Impedance Spectroscopy: Theory, Experiment and Applications*, ed. E. Barsoukov and J. R. Maconald, John Wiley & Sons, Inc., Hoboken, New Jersey, 2nd edn, 2005, pp. 27–128.
16 D. R. Crow, in *Principles and Applications of Electrochemistry*, Chapman and Hall, New York, 3rd edn, 1984, pp. 166–171.
17 H. C. Chang and G. Jaffe, *J. Chem. Phys*., 1952, **20**, 1071–1077.
18 M. Kato, *J. Theor. Biol*., 1995, **177**, 299–304.
19 D. E. Goldman, *J. Gen. Physiol*., 1944, **27**, 37–60.
20 J. Pellicer, V. M. Aguilella and S. Mafe, *J. Membr. Sci*., 1986, **29**, 117–126.
21 V. V. Kharton and F. M. B. Marques, *Solid State Ionics*, 2001, **140**, 381–394.
22 T. R. Brumleve and R. P. Buck, *J. Electroanal. Chem*., 1978, **90**, 1–31.
23 C. R. Paul, in *Fundamentals of Electric Circuit Analysis*, John Wiley & Sons, New York, 2001, pp. 13–28.
24 Z. P. Shao and S. M. Haile, *Nature*, 2004, **431**, 170–173.
25 M. Mogensen, N. M. Sammes and G. A. Tompsett, *Solid State Ionics*, 2000, **129**, 63–94.
26 W. Lai, Ph. D. Thesis, California Insitute of Technology, 2007.
27 T. A. Davis, *ACM Trans. Math. Software*, 2004, **30**, 165–195.
28 T. A. Davis, *ACM Trans. Math. Software*, 2004, **30**, 196–199.
29 T. A. Davis and I. S. Duff, *SIAM J. Matrix Anal. Appl*., 1997, **18**, 140–158.
30 T. A. Davis and I. S. Duff, *ACM Trans. Math. Software*, 1999, **25**, 1–20.
31 B. A. Boukamp, *Solid State Ionics*, 2004, **169**, 65–73.